DOI: 10.1002/anie.201406096

Micro- and Nanomotors

Chemically Powered Micro- and Nanomotors

Samuel Sánchez, Lluís Soler, and Jaideep Katuri*

Keywords:
catalysis · micromotors · nanomotors · robots · self-propulsion

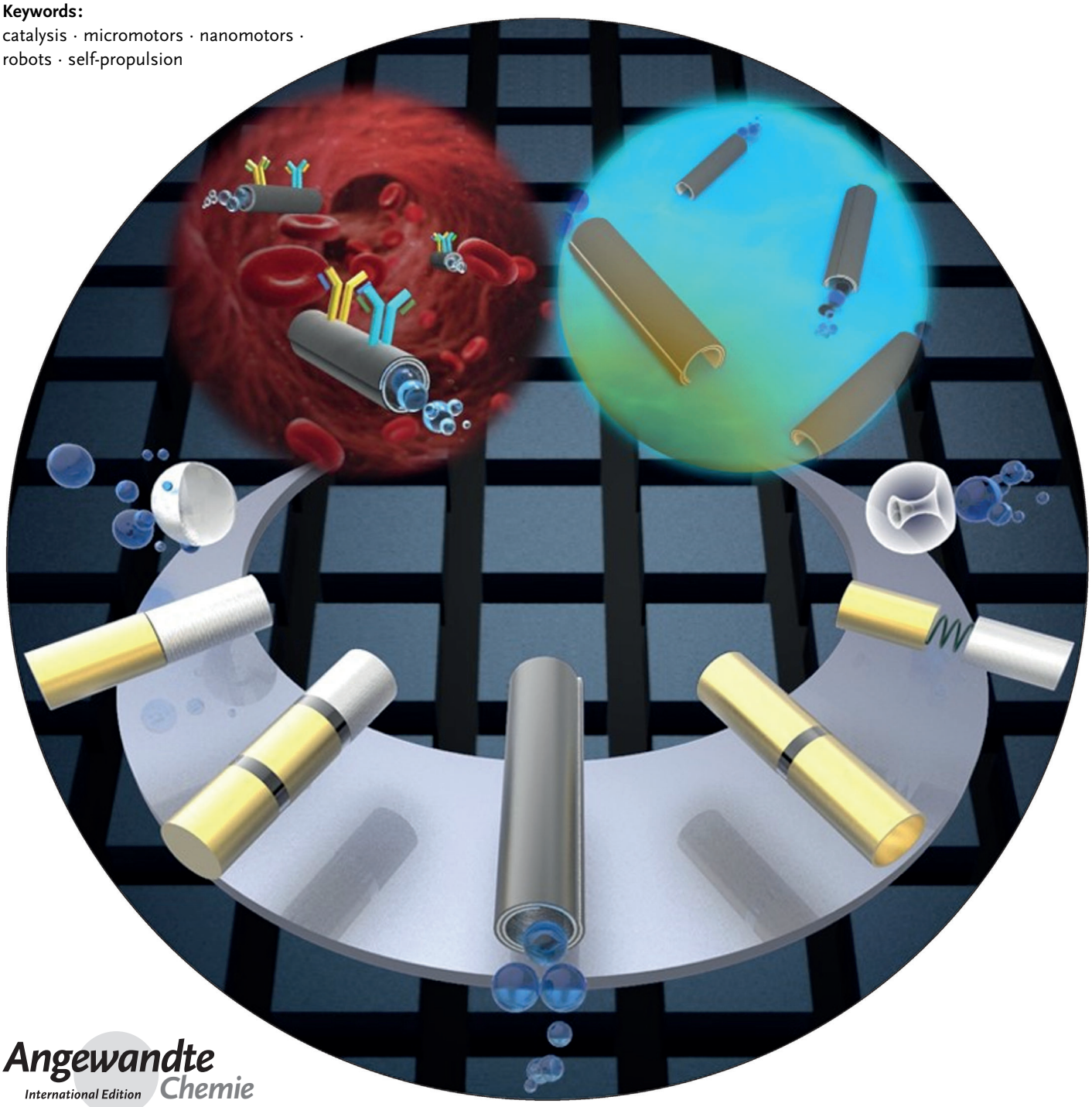

Angewandte International Edition Chemie

Chemically powered micro- and nanomotors are small devices that are self-propelled by catalytic reactions in fluids. Taking inspiration from biomotors, scientists are aiming to find the best architecture for self-propulsion, understand the mechanisms of motion, and develop accurate control over the motion. Remotely guided nanomotors can transport cargo to desired targets, drill into biomaterials, sense their environment, mix or pump fluids, and clean polluted water. This Review summarizes the major advances in the growing field of catalytic nanomotors, which started ten years ago.

From the Contents

1. Introduction

Chemically powered micro- and nanomotors (MNMs) are small autonomous devices capable of performing complex tasks while being self-propelled in fluids. They have the potential in the near future to revolutionize emerging topics in multidisciplinary nanotechnology, medicine, sensing, and environmental science. Ten years after the pioneering studies on catalytic nanomotors, which were reported independently but almost simultaneously by research groups at Penn State University and Toronto University,[1] the field has grown exponentially from the fundamental understanding of motion mechanisms and motion control, to proof-of-concept applications in different fields. Those artificial nanomotors had a larger precedent—on the centimeter scale—in the "catalytic boat" developed by a team at Harvard University in 2002.[2] More self-propelled macroscopic motors, which range from millimeters to centimeters in size, were later developed.[3]

Whether inspired by biological motors,[4] science fiction (with movies such as "Fantastic Voyage"), or by the visionary speech from Richard Feynman,[5] the results achieved over the last decade in man-made nanomachines have certainly reached limits beyond those imagined in "Dream Nanomachines", an inspiring and early review on the topic.[6]

Motion at the nanoscale is, however, one of the grand challenges of multidisciplinary nanotechnology and chemistry. On scaling machines down, factors such as viscosity and Brownian diffusion make motion of those tiny machines a difficult task. To achieve continuous motion in those regimes, MNMs can be externally actuated by a macroscopic device that provides energy, mainly an electric,[7] a magnetic,[8] or an acoustic field,[9] which is converted into motion. Self-propelled MNMs can also be autonomous, such as biomotors, which obtain mechanical energy from in situ chemical reactions through the use of catalysts. This is what we define as "chemically self-powered MNMs". The generated mechanical work allows these motors to move through a fluid phase while simultaneously or sequentially performing a task or series of tasks.

Here, we present an overview on the current state of synthetic catalytic nanomotors, with the aim of showing that the dream presented 10 years ago is much closer to reality today than had been expected. We describe the main fabrication methods for MNMs, with the aim of promoting the field to scientists of different disciplines and various infrastructure possibilities. We discuss the theoretical propulsion mechanisms of each type of motor and summarize the ways to provide motion control. Synthetic MNMs are very attractive micro- or nanodevices, because in addition to their fundamental relevance, they have demonstrated their functionality in several applications, ranging from drug delivery to environmental remediation. MNMs can act individually as well as collectively. Although this Review will focus on individual MNMs, we consider the collective behavior of MNMs and their coordinate motion as a very interesting phenomenon, which has recently been modeled theoretically[10] and demonstrated experimentally.[4g,11] We believe that the state-of-the art on this topic deserves a fully dedicated review, which cannot be covered herein.

Despite the significant and fast advances in the field, challenges still remain to find specific relevant (bio) applications, biologically compatible fuels, and more efficient mechanisms.[12] Moreover, improved geometries and fabrication methods are needed. We expect that synergy between nanotechnological tools for fabrication and biomedical imaging will play an important role in the near future.

1.1. Reynolds Numbers and Brownian Diffusion: The Challenges at the Nanoscale

MNMs operate in a regime where the outcome of physical laws is significantly different from the one in which we live. At the MNM scale, the effect of viscous drag and Brownian randomization has a determinant effect on motion. The Reynolds number (Re) is a dimensionless quantity which relates to the ratio of the inertial forces to viscous forces and is given by Equation (1).

[*] Dr. S. Sánchez, Dr. L. Soler, J. Katuri
Max Planck Institute for Intelligent Systems
Heisenbergstrasse 3, 70569 Stuttgart (Germany)
E-mail: sanchez@is.mpg.de
Homepage: http://www.is.mpg.de/sanchez
Dr. S. Sánchez
Institute for Bioengineering of Catalonia (IBEC)
08028 Barcelona (Spain)
and
Institució Catalana de Recerca i Estudis Avançats (ICREA), 08010 Barcelona (Spain)

$$\mathrm{Re} = \frac{\mathrm{p}Vl}{\mu} = \frac{\text{Inertial Forces}}{\text{Viscous Forces}} \quad (1)$$

Here, ρ is the density of the fluid, V is the velocity of the particle, l is the characteristic length of the object, and μ is the dynamic viscosity of the medium.[13] A high Re number corresponds to a system where inertial forces dominate over viscous forces, such as the macroscopic world, while at the smaller length scales of bacteria and MNMs, where viscous forces largely dominate, the Re number is low. To put this into perspective, a person swimming in water has a Re number of about 10^4, while a swimming bacterium has a Re number of 10^{-4}.

At low Re numbers, inertia can no longer sustain motion, as any motile force applied is immediately counteracted by the viscous drag. The system reaches its terminal velocity quickly and contains no momentum. MNMs hence have to be designed to create instantaneous (constant) force to generate continuous motion. The movement of these motors also has to be nonreciprocal. The conventional back and forth movement that is used to generate motion with high Re numbers can no longer be used for MNMs, as no net directional motion can result from it, as summarized in the "scallop theorem".[13] Therefore to induce motion, time reversal symmetry has to be broken, which adds significant complication to the design of MNMs.

Brownian motion is the random motion of the particles caused by the thermally driven collisions of solvent molecules with the colloidal particles. Brownian diffusion is characterized by the diffusion coefficient D, which is defined by the Stoke–Einstein relationship [Eq. (2)].

$$D = {k_\mathrm{B}T}/{6\pi\eta r} \quad (2)$$

Here, k_B is the Boltzmann constant, T is the absolute temperature, η is the viscosity, and r is the radius of the particle. The diffusion coefficient is related to the thermal energy of the system and the size of the particle. As the particle size decreases, Brownian motion significantly interferes with the directionality of the motors, thereby leading to random motion and reorientation. Thus, remote control over the motion of MNMs is a very important aspect to consider when designing artificial MNMs.

1.2. Bio-Inspired Nanomotors

Nature provides examples of highly efficient biological motors that perform complex tasks autonomously by converting chemistry into motion. Examples include cell division, DNA transcription, protein synthesis, and cell migration.[14] Synthetic MNMs try to mimic their biological counterparts by using simple engineered microstructures, which will enable small steps to be made towards the understanding, optimization, and applications of nanomotors.

Biomotors are classified into two groups: linear and rotary motors. Typical examples of linear motors are the motor proteins kinesins and dyneins—transporters of vesicles and molecules along microtubules—and myosins—which are responsible for muscle contraction and which move along actin filaments. Biomotors exploit catalysts to convert chemical energy (usually the hydrolysis of adenosine triphosphate, ATP) into the required mechanical output. For example, kinesin moves in small steps (8 nm)[15] from the minus end to the plus end of microtubules upon hydrolysis of ATP, and is responsible for the transport of cargo and delivery within the cell.[16]

F_0F_1-ATP synthase is a membrane protein rotary motor that uses electroosmotic energy from a proton or sodium gradient to synthesize ATP from adenosine diphosphate (ADP) and inorganic phosphate. Rotary motor ATPase converts chemical energy into electrochemical energy, which provides the rotation of flagella in some bacteria.

1.3. Hybrid Micro-Biorobots and Motors

Hybrid micro- and nano-biomotors integrate biological and synthetic components to synergistically improve individual performances. Motor proteins have been integrated in vitro into nanopatterned devices for the active transport of biological and inorganic cargo[17] as well as nanofluidics.[18] They can be used as nano-biosensors[19] and nanoscale probes to examine surfaces, and have been suggested as nanofluidic pumps (Figure 1 A).[20] Swarms of "molecular shuttles" have also been observed to modify the diffusion flows in nanofluidic devices.[21]

Single enzymes such as urease can act as nanomotors, as indicated by an enhancement in the diffusion coefficient in

Lluís Soler was born in Terrassa (Spain) in 1979. He received his PhD in chemistry from the Autonomous University of Barcelona (UAB) in 2010. 2010–2012 he was a Senior Researcher with the UAB in the testing of a new hydrogen generation prototype. In 2012 he joined the Leibnitz Institute for Integrative Nanoscience, Dresden (Germany), as a Postdoctoral Research Fellow. He is currently at the MPI for Intelligent Systems, Stuttgart (Germany). His research interests include self-propelled micro- and nanomotors, fabrication of nanomembranes, hydrogen generation, hydrogen storage, and fuel cells.

Samuel Sanchez received his PhD in chemistry from the Autonomous University of Barcelona (Spain) in 2008. In 2009 he joined the International Research Center for Materials Nanoarchitectonics, National Institute for Materials Science, Tsukuba, Japan. Since 2010 he has led the "Biochemical Nanomembranes" Group at the Institute for Integrative Nanosciences (IIN), Leibniz Institute for Solid State and Materials Research (IFW), Dresden (Germany). He is currently group leader at the MPI for Intelligent Systems, Stuttgart (Germany). His main interests are nanorobotics, biophysics, and integrated biosensors.

the presence of urea (Figure 1 B.b).[22] The enzyme catalase shows enhanced diffusivity as a result of substrate turnover in microfluidic devices, where a gradient of substrate concentration is accurately generated to induce chemotaxis of enzymes. Urease and catalase show collective movement towards higher substrate concentrations.[30]

Enzymes can be coupled to artificial components and provide motion or rotation to micro- or nanodevices. Montemagno and co-workers coupled F_1-ATPase to a Ni wire post, which rotates when Na_2ATP is added as a substrate and stops on addition of NaN_3.[31] Mano and Heller coupled glucose oxidase (GOx) and bilirubin oxidase to a carbon fiber suspended at the air–liquid interface. This fiber moved by bioelectrochemical propulsion when glucose was present in the solution.[32] Feringa and co-workers found that coupling GOx and catalase to carbon nanotubes results in the formation of bubbles in the presence of glucose and oxygen (O_2).[33] However, no directional motion was clearly observed. Although the use of glucose as a fuel to propel micromotors in a controlled manner has been hypothesized, its exploitation has not been achieved. As a first step, Sanchez et al. integrated the highly efficient enzyme catalase into microtubular structures through the use of self-assembled monolayers (SAMs; Figure 1 B.a).[24] The self-propelled microjets generate O_2 bubbles from the decomposition of hydrogen peroxide (H_2O_2) more efficiently than Pt-based microjets. A similar approach was later used by Orozco et al.[34] and Simmchen et al.[35] to couple catalase to template-based microjets and Janus particles, respectively. The hybrid motors found applications in the detection of heavy metals in water[34] and coupling of DNA.[35]

Motile cells and artificial parts are also interesting hybrid micromotors which could have relevance in future medical applications.[36] Several research groups have bound bacteria to microparticles[25,27] (Figure 1 C.a,b,e) and other microstructures such as microgears (Figure 1 C.c,d)[26,37] and studied their motion as microcarriers in vitro and in improved cargo-binding events.[38] Magnetic resonance imaging (MRI) has been used by the Martel research group to control in real time the motion of magnetic particles and magnetotactic bacteria with the aim of developing hybrid nanorobots for transporting cargo in the human body.[39]

In a recent and medically relevant study, single bovine sperm were encapsulated into conical magnetic microtubes (Figure 1 C.f).[28] The motile cells provide the driving force for the micro-biorobot, which can be remotely guided by an external magnetic field. Parker and co-workers presented a hybrid jellyfish by developing a polydimethoxysiloxane (PDMS) structure that was coated with micropatterned muscle cells, which allow contraction of the swimming jellyfish (Figure 1 C.g).[29] Hybrid microdevices such as pumps can also be engineered by using molecular motors,[20] enzymes,[40] swimming bacteria,[41] and other cells.[42] The combination of biological motors and artificial microdevices could be one of the most promising synergies for future microrobotics with full biocompatibility.

Jaideep Katuri received his BSc (Hons) in Physics from Sri Sathya Sai Institute of Higher Learning, Bangalore. He then joined the University of Stuttgart to pursue his Masters in Physics. Currently he is a student assistant at the research group of Samuel Sanchez at the MPI for Intelligent Systems in Stuttgart. His research focuses on studying the behavior and interactions of micromotors at different interfaces.

2. MNMs: From Fabrication to Motion Control

In the following section, we present the common methods for fabricating the three main geometries of artificial chemically powered MNMs, namely nanowires, Janus spheres, and microtubes. We discuss the mechanisms of motion described in the literature and the ways to control the motion. Externally actuated MNMs will be briefly presented.

2.1. Nanowires

Since the early 1970s, an impressive number of methods have been developed to grow metal nanostructures.[43] The growth of metal nanowires in hard templates was first reported in 1970 by Possin, who electroplated nanowires of Sn, In, and Zn into pores formed by etching out damage tracks produced in mica by high-energy charged particles.[44] Single metal nanowires in alumina membranes were first produced by Maskovits and co-workers in 1994,[45] but lack the asymmetry that has since been found to be essential for catalytic nanomotors. The initial methods to fabricate bimetallic and striped nanomotors were described by Mallouk and co-workers[46] in 1999 and by Natan and co-workers in 2001,[47] but the first application of Pt/Au bimetallic nanowires as catalytic motors was not reported until 2004 by Paxton et al.[1a]

2.1.1. Fabrication of Nanowires: Rigid, Striped, and Flexible

Research in the field has resulted in track-etched anodic alumina (AAO) membranes and polycarbonate (PC) containing cylindrical or conical pores becoming established as the preferred templates for the growth of nanowires by electrodeposition (Figure 2 A–C),[45,48] both of which are now produced commercially. In a typical experiment to produce metallic nanowires, the branched side of the membrane is coated with Ag/Au to act as a working electrode, a Pt wire is used as a counter electrode, and an Ag/AgCl electrode is employed as a reference electrode. The structure of each nanowire is controlled by the diameter of the membrane pore, which sets the width and the charge passed in each step, and thus dictates the length of the nanowire. With noble metals such as Ag, Au, Pd, and Pt, the growth of the nanowires is not complicated by oxide formation; however, the oxide layer is

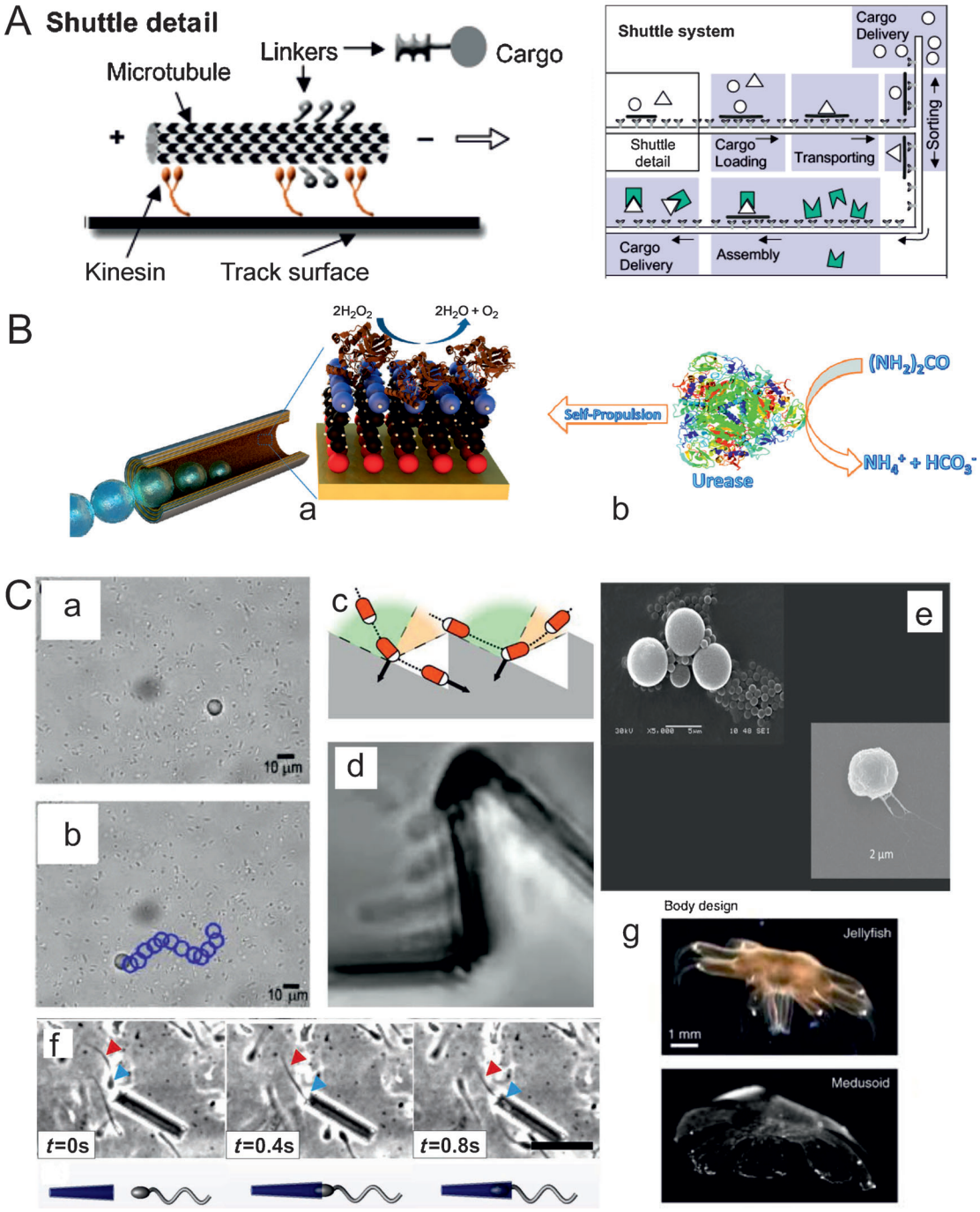

Figure 1. Hybrid micro-biomotors combining biological and synthetic parts. A) Molecular motors, which combine synthetic environments and biomotors, as shuttles for cargo loading, transport, and delivery. B) Enzymes used for self-propulsion. a) Microtubes coated with catalase for movement in H_2O_2 solutions and b) single urease molecule self-propelled in the presence of urea. C) Bacterial microrobotics attached to microparticles (a,b) which collide with microgears (c,d); e) flagellated magnetotactic bacteria attached to microbeads; f) coupling of a spermatozoon inside microtubes (scale bar 50 µm), g) composed of polymer and motile cells derived from jellyfish (top) and medusoid (bottom). Reprinted from Ref. [23] (A), Ref. [24] (B.a), Ref. [22] (B.b), Ref. [25] (C.a,b), Ref. [26] (C.c,d), Ref. [27] (C.e), Ref. [28] (C.f), Ref. [29] (C.g) with permission.

difficult to avoid with metals such as Zn, Sn, Cu, and Pb. Sequential deposition of different metals is used to form bimetallic nanowires or striped nanostructures. The sequence by which metal ions are introduced into solution defines the number and pattern of the metal stripes. In standard procedures, the nanowire-filled membranes are immersed in HNO_3 to dissolve the sacrificial layer and then immersed in NaOH to dissolve the AAO membrane. The nanowires are then centrifuged and rinsed in deionized water to remove the remaining NaOH. This method of fabrication or a version of it

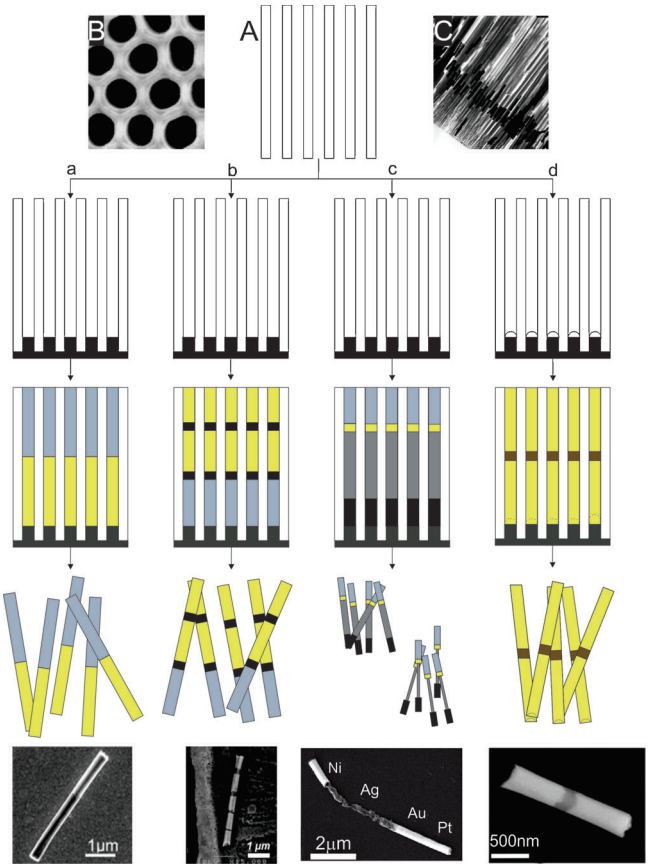

Figure 2. Preparation of nanowires. Nanowires can be produced by electrodeposition of metals into AAO or PC templates. A) A gold or silver layer is deposited on one side of the membrane to act as a working electrode. B) An AAO membrane used as a template for deposition. C) TEM image of an AAO template showing Au nanofibrils. a,b) Bimetallic and striped nanowires are produced by sequential deposition of metals into the template, where the charge controls the length of each segment. c) Flexible nanowires can be fabricated by depositing a Ag segment that can be partially etched after the deposition. d) Nanosphere lithography is used for fabricating wires with concave edges for propulsion by ultrasound. After deposition, the membrane is chemically dissolved and the wires are centrifuged out of the solution. Scanning electron microscopy (SEM) images reprinted from Ref. [48] (C), Ref. [49] (B), and Refs. [9c, 47, 50, 51] (A.a,b,c,d) with permission.

has since been used consistently for the fabrication of nanowire-based nanomotors (Figure 2 A.a,b).

A new class of flexible nanostructures was introduced by Ozin and co-workers in 2007.[52] These were metallic nanowires with polyelectrolyte hinges that were synthesized by using layer-by-layer electrostatic self-assembly of oppositely charged polyelectrolytes on striped metal nanowires followed by segment-selected chemical etching (Figure 2 A.c). These nanowires showed considerable flexibility, which depended on the number of bilayers. They were, however, not used for self-propulsion; only their structural properties were studied and the magnetic actuation of the bending motion was demonstrated. In 2011 Wang and co-workers used flexible multi-segment Pt/Au/Ag_{Flex}/Ni nanowires to demonstrate chemically powered propulsion and magnetically driven locomotion (Figure 2 A.c).[51] The formation of the hybrid nanowire motors involved a sequential deposition of the Au, Ag, and Ni segments into the AAO. Subsequent dissolution of the template and release of the nanowires was followed by partial dissolution of the central Ag segment in H_2O_2 to create the flexible thin Ag joint that links the Au and Ni parts (Figure 2 A.c). The flexible part is essential for controlled mechanical deformation, while the Ni part is used for magnetic control.

Besides the catalytically powered nanowires, there has been significant effort towards directing their motion by self-acoustophoresis (see Section 2.1.4). Levitation, propulsion, and assembly of these shape-asymmetric particles were demonstrated by Mallouk and co-workers in 2012.[9a] These shape-asymmetric metallic wires are typically composed of Au/Ru or Au/Ni/Au segments with a concave end (Figure 2 A.d). The Ni segment facilitates magnetic control, the Au segments make it convenient for functionalization, and the concave shape scatters the acoustic waves, thereby causing axial propulsion. Two separate methods have been used to achieve the concave shape in these nanowires. A Cu sacrificial layer is initially electrodeposited and is etched, which ultimately gives rise to a concave end. The concavity in this method, however, is not controlled. Wang and co-workers have proposed using polystyrene nanospheres as a sacrificial layer in the template to allow for more controlled concavity, and have demonstrated higher speeds using the samples fabricated by this method.[9c]

2.1.2. *Propulsion Mechanisms of Chemically Propelled Metallic Nanowires*

Ever since the autonomous motion of Au/Pt nanowires was demonstrated in 2004,[1a] the mechanism that causes the directional force has been a subject of much debate. Whitesides and co-workers moved millimeter-scale objects by using platinum (Pt) covered porous glass segments on PDMS surfaces, and attributed the movement of their microrobot to the recoil force of the O_2 bubbles released from the Pt catalyst.[2] A similar mechanism was suggested for Ni/Au nanowires, in which the Au end was anchored to a silicon wafer, which showed rotational motion on addition of H_2O_2.[1b] The authors claimed that asymmetric evolution of O_2 was causing the rotational motion (Figure 3 A). When this mechanism was tested in Au/Pt nanowires, it was noticed that the nanowires moved in the direction opposite to what was

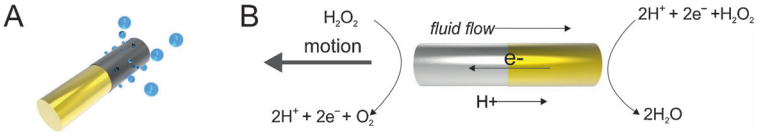

Figure 3. The two main proposed mechanisms for the motion of self-propelled nanowires: A) bubble propulsion of a Au/Ni nanowire and B) electrokinetic mechanisms of Pt/Au nanowires. Adapted from Ref. [6] (A) and Ref. [4a] (B).

expected, with the Pt end forward.[53] The macroscopic bubbles could no longer explain the motion of the nanowires. An alternative interfacial tension model was proposed on the basis of the idea that the O_2 generated in the decomposition of the fuel lowers the interfacial tension between the solution and the nanowire.[1a] Another model was built based on the Brownian ratchet mechanism.[54] Here, the O_2 formed at one end of the rod was described as causing a drop in the viscosity in the vicinity of the Pt, thereby enabling thermal motion to preferentially propel it in that direction.

However, the mechanism that has the strongest experimental evidence and largely accepted in the community is self-electrophoresis. The different mechanisms have been summarized in previous reviews.[4d,g,55] In self-electrophoresis, the charged microparticles migrate in a self-generated electric field as a result of an asymmetric distribution of ions. The velocity (U) of the particle is related to the electric field (E), zeta potential (ζ_{rod}) of the particle, viscosity (μ), and permittivity of the medium (ε) through Equation (3).

$$U = \xi_{rod}\varepsilon E/\mu \quad (3)$$

In the case of the bimetallic Au/Pt nanomotors, the oxidation of H_2O_2 occurs preferentially at the Pt end and the reduction of H_2O_2 at the Au end. Since there is an excess of H^+ on the Pt side, an electric field points from the Pt end to the Au end, and the negatively charged rod moves with the Pt side forward (Figure 3B).

In experiments conducted by Sen and co-workers it was noticed that an electrical contact between the Au and Pt ends was essential for propulsion, thus ruling out the interfacial tension model, which should be unaffected by this.[50] To confirm the mechanism the same research group plotted the Tafel plots of the anodic and cathodic H_2O_2 potentials at various metal (Au, Pt, Rh, Ni, Ru, and Pd) ultramicroelectrodes.[50] These measurements enabled the direction of motion of various metal combinations to be predicted by assuming a self-electrophoretic mechanism. These predictions were found to be consistent with experimental observations. By incorporating carbon nanotubes (CNTs) into the Pt end, Wang and co-workers demonstrated enhanced speeds, which was attributed to an enhanced electron transfer caused by the addition of the CNTs,[56] a phenomenon that is commonly observed in electrochemistry and biosensing. Further confirmation of the mechanism came when the same research group demonstrated enhanced speeds by using an Ag/Au alloy instead of the Au segment.[57] Ag/Au alloys have been shown to enhance electron-transfer reactions of H_2O_2 compared to Au or Ag alone, with an electrokinetic mechanism explaining the higher speeds. Although the H^+ gradient is responsible for the motion of bimetallic motors in H_2O_2 solutions, other fuels such as hydrazine, dimethylhydrazine,[58] as well as dilute I_2 and Br_2[59] solutions have been used to propel motors by the same mechanism involving electrokinetic flows similar to the ones observed in H_2O_2 system.

In 2011, Fattah et al. demonstrated nanowires that moved by the bubble propulsion mechanism.[60] They used a procedure based on bipolar electrochemistry to prepare carbon nanowires modified in a dissymmetric way with a platinum catalyst. In the peroxide solution, the bubbles generated from the platinum cluster could propel these wires and a switch between translational and rotational motion could be achieved by changing the symmetry of the Pt cluster.

2.1.3. Motion Control of Chemically Propelled Nanowires

Conceivable applications for these motors involve a precise temporal and spatial control of the motion, regulation of the motor speed either by controlling the motor activity or the fuel supply, and an on-demand on/off control. In the following sections various approaches to meet this challenge of directional and speed control will be reviewed (Figure 4).

2.1.3.1. Magnetic Control

The most common approach for gaining directional control of the nanoscale motors is by the use of external magnetic fields. Ferromagnetic (Ni, Fe) segments that are shorter in length than their diameter are incorporated into the nanowires so that they can be magnetized transversely, thus allowing for control of their orientation.[61] While the

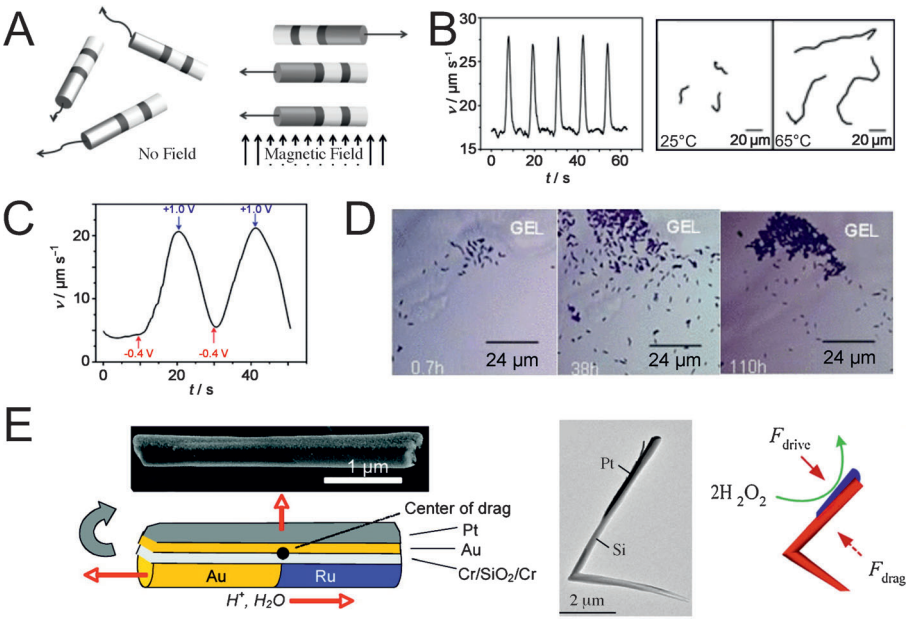

Figure 4. External methods for controlling the motion of catalytic metallic nanowires. A) Magnetic, B) thermal, C) electrochemical, D) chemical, E) design. Reprinted from Ref. [4d] (A), Ref. [62] (B), Ref. [63] (C), Ref. [11f] (D), and Ref. [11a, 65](E) with permission.

magnetic fields are used only for directional control and not as a propulsion mechanism, experiments with alternating strong and weak magnetic fields have demonstrated "stop and go" abilities. Sen and co-workers used (Pt/Ni/Au/Ni/Au) rods to demonstrate precise directional control over the nanorods in free fluids.[61a] The authors noticed that the magnetic field does not alter the speed of the particles, only the direction. Wang and co-workers demonstrated precise motion of Au/Ni/Au/Pt-CNT particles in complex microchannel systems.[61b] Besides directional control, fast shifting magnetic fields are also used for the capture and release of cargo, a promising application in lab-on-a-chip devices, which will be covered in detail in Section 3.1 (Figure 4A).

2.1.3.2. Thermal Control

Short heat pulses have been used to regulate the speed of nanomotors. Pt/Au nanowires subjected to elevated temperatures were found to travel significantly faster than those at room temperature. For example, an average speed of 45 $\mu m\,s^{-1}$ was observed for nanowires at 65 °C compared to 14 $\mu m\,s^{-1}$ at 25 °C.[62] This increase in speed was attributed to the temperature dependency of the electrochemical process and the reduction in the solution viscosity. The application of heat pulses is a highly reversible process and when combined with magnetic guidance enables a more advanced temporal and spatial control, with the capacity to manipulate both the speed and direction (Figure 4B).

2.1.3.3. Electrochemically Triggered Motion

The electrochemically controlled movement of catalytic nanomotors was demonstrated by Wang and co-workers.[63] By stepping the potential of a Au electrode placed near the nanowires in a bulk solution from negative to positive values, they could control the speed of the nanowires. Stepping the potential from −0.4 V to different positive potentials led to a steady decrease in the speed from nearly 20 $\mu m\ s^{-1}$ to 16, 10, and 4 $\mu m\ s^{-1}$ (at +0.40, +0.60, and +1.0 V, respectively). The process was also reversible, with faster speeds being induced by increasing the negative potentials. This potential-induced motion control has been explained to be due to changes in the local level of O_2, which is generated and consumed at the positive and negative potentials, respectively (Figure 4C).

2.1.3.4. Chemically Controlled Nanomotor Movement

Chemotaxis is the movement of organisms toward or away from a particular chemical attractant or toxin by a biased random walk process. Sen and co-workers published experimental evidence of chemotaxis in nonbiological systems containing Pt/Au nanowires, where H_2O_2 acted as the attractant.[11f] The authors observed a random walk motion of 2 μm long Pt/Au wires in H_2O_2 solutions. In a gradient of H_2O_2, the motion has a slight bias directed toward higher H_2O_2 concentrations. It is also well-known that the speed of the nanowires increases linearly with the H_2O_2 concentration over the range 2.5–10 wt%.[56] Controlling and modulating the local fuel levels may lead to spatial manipulation of the speeds of particles. Wang and co-workers reported an increase in the speed of nanomotors from 50 to 94 $\mu m\,s^{-1}$[56] upon addition of hydrazine to the H_2O_2 fuel, and of the nanowire on addition of Ag ions to the H_2O_2 fuel.[64] Such an Ag-induced acceleration was credited to the underpotential deposition of Ag on the Au/Pt nanowires leading to differences in the surface and catalytic properties (Figure 4D).

2.1.3.5. Motion Control by Design

Although the methods covered so far can be used for precise control of the direction and speed, more complex movement patterns become necessary for advanced applications. A rotational component of the motion can be achieved by imparting an asymmetric geometry into the nanowires. The Zhao research group used a geometric shadowing effect to coat a thin layer of a catalytic layer asymmetrically on the side of a nanowire.[65] On addition of H_2O_2, these nanowires rotated around a fixed point near their end. The random orientations of the nanowires in the solution led to both clockwise and counterclockwise rotations being observed. The authors further fabricated L-shaped nanowires, by combining the geometric shadowing effect with substrate rotation, which also showed rotational motion from the long arms to the short arms. The Mirkin research group used on-wire lithography to asymmetrically coat the nanowires and thus expose the catalytic surface only on one side,[66] thereby allowing the nanowires to rotate in H_2O_2. Mallouk, Sen, and co-workers vapor-deposited additional layers of Cr, SiO_2, Cr, Au, and Pt on one side of Au/Ru bimetallic nanowires and showed rotations up to 400 rpm with an average of 180 rpm in 15% H_2O_2 solution[11a] (Figure 4E).

2.1.4. Externally Actuated Nanowires

One of the greatest challenges of nanomotor research is to develop motors that can operate in biocompatible media, which excludes the use of H_2O_2 as a fuel source. Externally actuated motors are promising in this aspect, as they rely on nonchemical propulsion forces, which can potentially be safer for biomedical applications as no toxic chemicals are needed as a fuel for propulsion. Wang et al. reported nanowires that were propelled by ultrasonic energy, which at low power has been found to be safe and is used for in vivo imaging. These nanowires were driven by a frequency in the MHz range and achieved speeds up to 200 $\mu m\,s^{-1}$.[9a] Self-acoustophoresis (motion of a particle in an accoustic field gradient as a result of its symmetry) was proposed as the propulsion mechanism on the basis of the observation that the nanowires moved from the concave end to the convex end. Asymmetric scattering of the ultrasound waves from the two geometrically different ends causes a pressure difference across the motor, thereby imparting an axial propulsion force. Wang and co-workers developed a sphere lithography method to control the concavity of the wires and demonstrated enhanced speeds.[9c]

Flexible nanowires can be propelled by an external rotating magnetic field. These motors have a Ni/Ag/Au composition, with the Ag segment being thin and flexible.

The flexible Ag segment facilitates a cone-shaped rotation of the Ni segment around the axis of the nanowire. This in turn causes a rotation of the Au end on the other side. The rotation of the Au and Ni segments at different amplitudes and with a phase difference, which is enabled by the bending of the flexible Ag part, breaks the system symmetry and causes motion.[51]

2.2. Spherical Micro- and Nanomotors

The term Janus beads was used for the first time in the pioneering studies by Casagrande et al. in 1988[67] to describe spherical glass particles with one of the hemispheres hydrophilic and the other hydrophobic. Three years later, De Gennes used the term "Janus grains" in his Nobel lecture.[68] Janus particles are named after the ancient Roman god Janus, usually depicted having two faces, because they are colloids with two sides of different physical and/or chemical properties. Since 1991, Janus particles have been prepared by a number of synthetic pathways and used in many applications.[69]

Rigid colloidal particles suspended in a solution could be propelled by gradients of solutes, as a result of interactions between the solute and the colloid surface, in a mechanism called diffusiophoresis.[70] When the suspended particles in a solution undergo chemical reactions on their surface, a gradient of reaction products is generated by the particles themselves, in a process termed self-diffusiophoresis. In 2005, Golestanian et al. proposed a simple model for the reaction-driven propulsion of a molecular machine in aqueous media, where the motion of the device was driven by an asymmetric distribution of the reaction products through a diffusiophoretic mechanism.[71] In 2007, the motion of artificial catalytic Janus particles was experimentally proven the first time by Golestanian and co-workers.[72]

The synthetic strategies towards the fabrication of spherical MNMs differ depending on the desired asymmetry, shape, and propulsion mechanism of the micromotor. Two main categories can be distinguished in terms of the MNM shape: spherical Janus particles and other spherical particles. In the first case, the surface of a spherical particle is half-coated with specific thin films that possess different physical and/or chemical properties from the uncoated surface of the particle. In the second case, a distinct class of MNMs emerges when the anisotropic surface coverage of the spherical particle is not restricted to a 50:50 ratio, which leads to self-propelled particles with one or multiple patches of varying surface, shape, and chemical properties. Here we summarize the fabrication methods of these two main classes of spherical MNMs.

2.2.1. Fabrication of Spherical Janus Motors

The most common technique to fabricate spherical Janus micromotors is based on the deposition of metallic thin films on microbeads to obtain half-coated particles (Figure 5A). For example, the deposition of a catalytic thin layer on the top of polystyrene (PS) or silica (SiO_2) microspheres leads to the

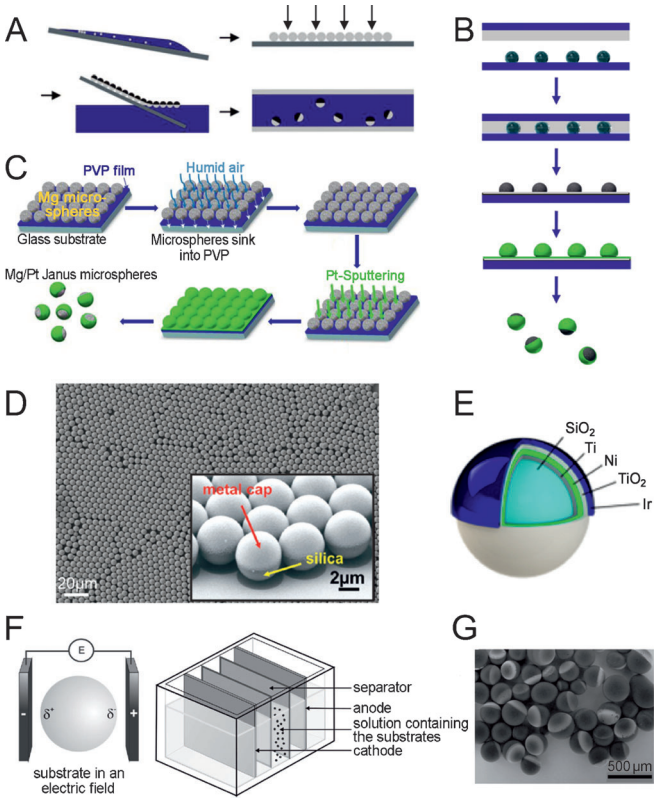

Figure 5. Fabrication of spherical Janus micromotors. A) Preparation of catalytic Janus particles. B) Fabrication of water-driven Al-Ga/Ti spherical micromotors. C) Fabrication of Mg/Pt Janus microspheres. D) SEM image illustrating an array of Janus microspheres. E) Multilayer $Ir/TiO_2/Ni/Ti/SiO_2$ Janus micromotor. F) Principle of bipolar electrochemistry and the cell used for bipolar electrodeposition. G) SEM image of glassy carbon beads with electrodeposited Au. Reprinted from Ref. [74] (A), Ref. [75] (B), Ref. [76] (C), Ref. [73] (D), Ref. [77] (E), and Ref. [78] (F,G) with permission.

fabrication of catalytic Janus micromotors, while the deposition of a metallic cap onto spherical Mg, Al, or Al alloy particles results in redox Janus micromotors that use the body of the motor as a fuel itself (Figure 5B,C). Typically, in the first step, a suspension of the selected particles in alcohol or water is drop-cast onto a cleaned substrate and dried uniformly to obtain a dense monolayer of the spheres (Figure 5D). Glass slides or Si wafers are commonly used as substrates.[73] Varying the concentration of particles in the colloid suspension, the size of the droplet to be spread onto the substrate, and the tilting angle of the substrate allows the density of the monolayer covering the substrate to be tuned. Thin metal layers are then evaporated onto the monolayer of particles by electron-beam evaporation or sputtering systems to obtain multimetallic half-caps on the top of the microspheres (Figure 5E). Finally, the particles are released from the substrate into the selected solvent by sonication and used.

Alternatively, bipolar electrochemistry can be used to produce catalytic spherical Janus particles.[78] In this particular case, conducting beads are required to allow metallic deposition on one of the polarized hemispheres, which results

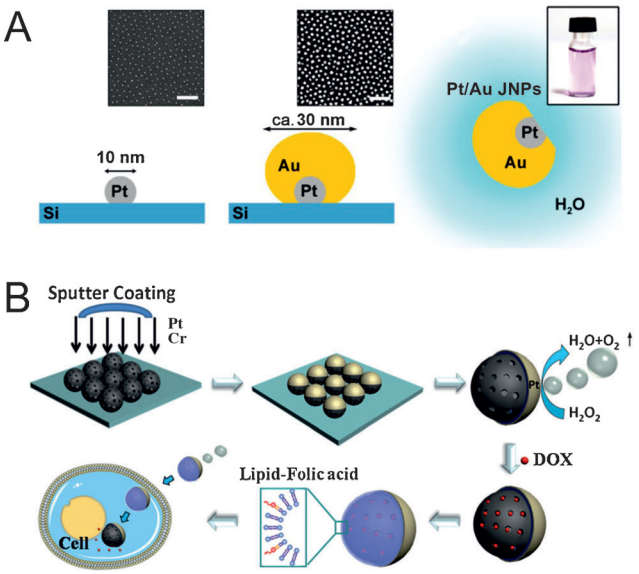

Figure 6. Fabrication of spherical Janus nanomotors. A) Schematic representation of the preparation of Au/Pt Janus nanomotors. Scale bar: 200 nm. B) Fabrication procedure for Janus MSN nanomotors, drug loading, lipid bilayer functionalization, and drug release. DOX = doxorubicin hydrochloride. Reprinted from Ref. [79] (A) and Ref. [82] (B) with permission.

in metallic half caps on the surface of conducting beads (Figure 1 F,G).

In 2014, Fischer and co-workers synthesized the smallest Janus nanomotors reported to date, with an overall size of about 30 nm.[79] The fabrication procedure is depicted in Figure 6 A. Briefly, an array of Pt nanoparticles (NPs) was produced by block copolymer micelle lithography[80] on a Si wafer. Then, Au was deposited onto the Pt NPs by glancing-angle deposition[81] (GLAD) under fast substrate rotation. Each individual Pt NP acted as a nanoseed for the deposition of Au vapor, thereby resulting in a Janus-type Au NP with an embedded Pt NP on one face. The geometry of the resultant Janus NPs (JNPs) can be controlled by the rotation speed, angle of incidence, and the deposition rate.

Parallel studies by Xuan et al. led to the synthesis of self-propelled Janus nanomotors with a diameter of about 75 nm.[82] The method of preparation is illustrated in Figure 6 B. Spherical mesoporous silica nanoparticles (MSNs) were synthesized according to a base-catalyzed sol-gel method.[83] Then, MSNs were spread on a Si wafer to form a monolayer and subsequently coated with evaporated Cr and Pt. A brief sonication led to the Janus MSNs becoming dispersed in a solution of the anticancer drug doxorubicin hydrochloride to load the cargo, and subsequent mixing with 1 mg mL^{-1} egg phosphatidylcholine containing 1 % folic acid led to encapsulation.

Table 1 summarizes the different fabrication methods for chemically self-propelled spherical Janus MNMs.

2.2.1.1. *Fabrication of Other Spherical Motors*

Recently, a collection of spherical catalytic MNMs was demonstrated that takes advantage of the anisotropy offered

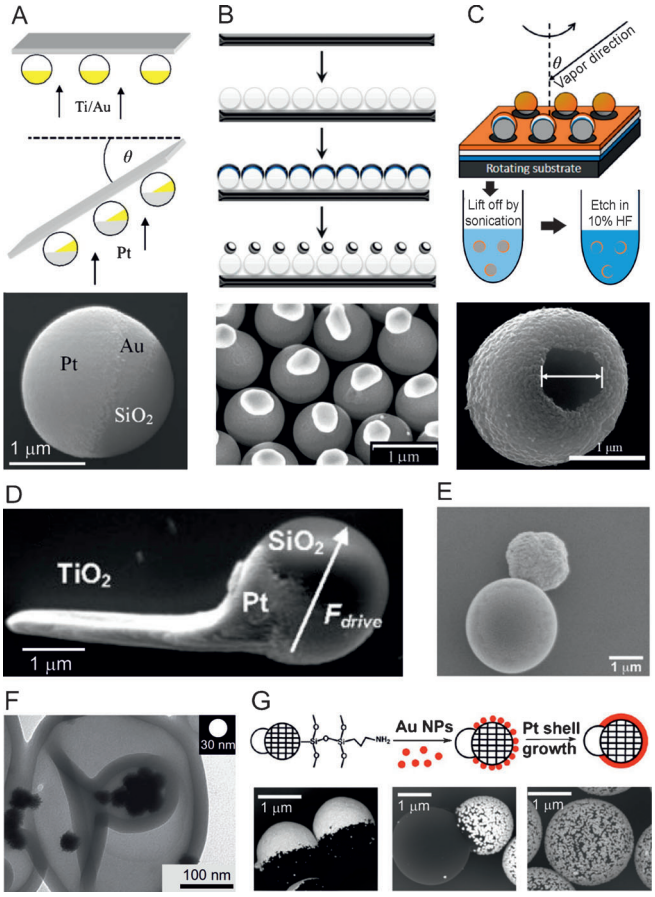

Figure 7. Fabrication of catalytic spherical MNMs. A) Preparation of asymmetric Pt/Au-coated catalytic micromotors. The SEM image shows an asymmetric Pt/Au micromotor with Pt deposited at $\theta = 40°$. B) Synthesis of the self-propelled spherical SiO_2-Pt dimers and representative SEM image. C) Fabrication procedure of nanoshell motors. The SEM image shows a representative image of a nanoshell motor. D) SEM image of a single tadpole micromotor. E) SEM image of a PS-Ag colloidal heterodoublet. F) SEM image of the entrapment of Pt NPs in polymer stomatocytes. G) Procedure for making Pt-PS hybrid dimers. Representative SEM images of Pt-PS Janus spheres, Pt-PS Janus dimmers, and Pt spheres uniformly coated with Pt NPs. Reprinted from Ref. [84] (A), Ref. [88] (B), Ref. [86] (C), Ref. [85a] (D), Ref. [89] (E), Ref. [91] (F), and Ref. [90] (G) with permission.

by expressly patterned particles and/or the assembly of colloidal building blocks. Zhao and co-workers used dynamic shadowing growth (DSG) deposition processes[65] to develop several fabrication methods for self-propelled objects, such as asymmetric-coated spherical particles (Figure 7 A),[84] tadpole-like micromotors (Figure 7 D),[85] V-shaped micromotors,[85a] and catalytic spherical nanoshells (Figure 7 C).[86] Tierno et al. reported the elongation of embedded PS particles in a poly(vinyl alcohol) matrix by using toluene and a subsequent Pt deposition on the top of the elongated particles to prepare self-propelled microellipsoids.[87]

In 2010, the research groups of Ozin and Sen reported the first examples of spherical silica-Pt dimers (Figure 7 B)[88] and colloidal PS-Ag and silica-Ag heterodoublets (Figure 7 E)[89] that undergo self-propulsion in aqueous H_2O_2 solutions. At the beginning of 2014, Wang et al. described a method to prepare spherical PS dimers and subsequently decorate one of

Table 1: Summary of chemically self-propelled spherical Janus MNM.

Mechanism of propulsion[a]	Particle/diameter [μm][b]	Metals/thickness [nm]	Fuel	Ref.
	PS/1.62	Pt/5.5	1–10% H_2O_2	[72]
	SiO_2/2–5; PS/n.a.	Ag/60–80	0.5% H_2O_2 + UV light	[89, 94]
	SiO_2/1	Pt/5	15.0–23.7% H_2O_2	[95]
	PS/2	Pt/5	10% H_2O_2	[96]
	fluorescent PS/1.99	Pt/5	5% H_2O_2	[97]
	SiO_2/0.96	Cr/7; Au/56; Gurbbs catalyst	0.01–0.5 M norbornene	[98]
	PS/0.5–10	Pt/n.a.	10% H_2O_2	[99]
	carboxylate PS/5	Ti/2; Pt/5	3–15% H_2O_2	[100]
	SiO_2/5	Pt/2–[Co/0.4-Pt/0.6]×5–Pt/15 Pt/1 [Co/0.3-Pt/0.8]×8–Pd/5	0–30% H_2O_2	[73, 101]
SDP	SiO_2/4.8	Ni, Pd, Pt, [Co/Pt]multilayer stack	3–7% H_2O_2	[74]
	SiO_2/5	Ti/2; Pt/15	10% H_2O_2	[11j]
	fluorescent PS/1.9–3.1–4.8	Pt/10	10% H_2O_2	[102]
	amberlite/300	PECA-PMMA[c]	1 M NaOH	[103]
	SiO_2/2.08–0.96	Pt/7	1.25–15% H_2O_2	[104]
	SiO_2/2	Pt/7	2.5–10% H_2O_2	[105]
	MSNPs/0.075	Cr/3; Pt/7	1–30% H_2O_2	[82]
	SiO_2/1.21–4.74; PS/0.91	For SiO_2 4.74: Ir/20 for SiO_2 1.21: Ir/10 for magnetic motor: Ti/10; Ni/15; TiO_2; Ir/10–20	10^{-7}–10% N_2H_4	[77]
	Au-Pt/0.03	Au-Pt/30	0.1–1.5% H_2O_2	[79]
SDP/SEP	SiO_2/4.78	[Co/0.4-Pt/0.6]×5–Pt/5	2.5–20% H_2O_2	[106]
	SiO_2/2	Pt/7	5% H_2O_2 + electric field	[107]
	fluorescent PS/5	Au/20 ×8;[d] Pt/20	1–4% H_2O_2	[108]
SEP	fluorescent PS/2	Pt/5	10% H_2O_2	[109]
	PS/2	Pt/10	10% H_2O_2	[110]
SDP/BP	PS/1–2	Pt/10 or Pt NPs	1–10% H_2O_2	[90]
	amberlite	Pd NPs[e]	5% H_2O_2	[111]
	SiO_2/2.01	Ti or Ni/0.5–0.8; Pt/50	0.5–0.7% H_2O_2	[112]
	Al/20	Ga; Ti/200	H_2O	[75]
	SiO_2/10–50	Ti/10; Pt/25	5% H_2O_2	[113]
BP	SiO_2/8	PSS-PAH[f]-Pt NPs/200	15% H_2O_2	[114]
	Mg/20	Pt/100	0.1–1 M $NaHCO_3$	[76]
	Mg/30	Ti/20; Ni/80; Au/10	seawater	[93]
	Al/5–30	Ti/50; Pd/300	acid/base/H_2O_2	[92]
	PS/16; SiO_2/4.8	reduced Ag	3% H_2O_2	[115]

[a] SDP = self-diffusiophoresis, BP = bubble propulsion, SEP = self-electrophoresis. [b] PS = polystyrene, MSNPs = mesoporous silica nanoparticles, n.a. = not available. [c] PECA = poly(2-ethyl cyanoacrylate), PMMA = poly(methyl methacrylate). [d] The particles were resuspended and Au deposition was repeated 8 times. [e] The particles were uniformly coated with Pd NPs. [f] PSS = polystyrene sulfonate, PAH = polyallylamine hydroclhoride.

the lobes with core–shell Pt@Au nanoparticles (Figure 7G), which can self-propel by using bubble propulsion.[90] Polymeric materials have been used to fabricate spherical nanomotors. Wilson et al. illustrated the fabrication of polymer stomatocytes loaded with Pt NPs, which exhibited autonomous motion in H_2O_2 solutions (Figure 7F).[91]

2.2.2. *Propulsion Mechanisms of Spherical Motors*

The propulsion mechanisms of spherical Janus particles have been the object of study in recent years. While it is clear that the motion of redox Janus particles driven by the Al-water[75,92] or Mg-water reactions[76,93] follows a bubble propulsion mechanism (Figure 8B), as evident by the observable generation and detachment of hydrogen (H_2) bubbles, the mechanism of the motion of the catalytic spherical Janus particles driven by decomposition of H_2O_2 remains a topic of debate. Besides bubbles, such as of H_2 or O_2, given off by chemical reactions, self-diffusiophoresis has been suggested as a propulsion mechanism for catalytic Janus particles suspended in a solution.[71,72] For example, PS-Pt Janus particles have been proposed as self-diffusiophoretic motors in H_2O_2 solutions,[72] where the decomposition of H_2O_2 on the

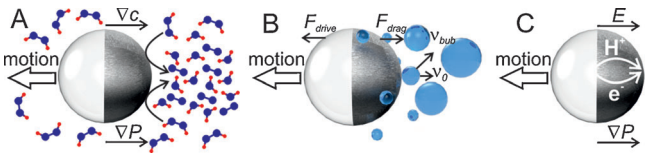

Figure 8. Different propulsion mechanisms driving the motion of self-propelled Janus Particles. A) Self-diffusiophoresis, where ∇c is a concentration gradient and ∇P is a pressure gradient. B) Bubble propulsion, where F_{drive} is the driving force, F_{drag} is the viscous drag force, v_{bub} is the bubble's velocity, and v_0 is the initial horizontal component of the velocity of a detached bubble. C) Self-electrophoresis, where E is an electric field and H^+ and e^- show the direction of flow of ions and the electric field, respectively. Adapted from Ref. [97] (A), Ref. [112] (B), and Refs. [4a, 109, 110] (C).

Pt surface generates solute gradients that drive the self-diffusiophoretic locomotion (Figure 8A). Nevertheless, other catalysts, such as dinuclear Mn complexes[116] and Ag- and MnO_2-based micromotors,[117] have also been used to propel spherical particles in the presence of H_2O_2, with the formation of O_2 bubbles driving the locomotion observed. The propulsion of catalytic self-propelled Janus particles as a function of H_2O_2 concentration,[72] spatial confinement,[118] transport of cargo,[100,119] particle shape,[120] and size[99] have been studied, both experimentally and theoretically, to support the self-diffusiophoretic mechanism. Nevertheless, more work is required to discover all the physicochemical factors that determine the locomotion of catalytic Janus particles in H_2O_2 solutions, for example, the experimentally observed effects of several ionic species on their swimming speed.[109,110] In a recent study, Brown and Poon suggested that the propulsion mechanism involved in the motion of PS-Pt Janus particles could be self-electrophoresis,[109] where an ionic current on the Pt surface generates a local electric field that acts on ionic gradients and drives the motion of the particle (Figure 8C). Parallel studies by Ebbens et al. illustrated experimentally and theoretically that electrokinetic effects can alter the motion of Pt-insulator Janus particles.[110] An ionic current passing between the pole and equator of the Pt half-cap could explain the ionic effects on the velocity of the Janus micromotors. This ionic current could be induced by asymmetries on the Pt surface or variation in the thickness of the half cap. However, the experimental data reported to date indicate that the mechanism of propulsion of catalytic Janus swimmers is considerably more complex than previously thought, and many other parameters may play a role, such as thermophoresis, Pt thickness and roughness, and the formation of invisible nanobubbles.[112]

2.2.3. Motion Control of Spherical Motors

The application of external magnetic fields to guide the motion of artificial micromotors is a frequently employed technique. Magnetic guidance of Janus particles can be achieved through the deposition of a ferromagnetic Ni layer (between 15 and 80 nm; Figure 9A).[77,93] Although Ni half-coated Janus particles have the ability to orient themselves in response to an external magnetic field, the high symmetry of the spherical shape cannot give a preferential orientation of the magnetic moment, because a Ni thin film presents an in-plane easy axis for magnetization. Consequently, the large-scale deterministic motion of spherical Janus particles guided by magnetic fields cannot be achieved by a simple magnetic monolayer deposited onto the cap of the microspheres. In a recent study, Baraban et al. reported an improvement in the magnetic guidance of spherical Janus particles,[73] in which they achieved an alignment of the magnetic moment along the main symmetry axis of the spherical Janus micromotor (Figure 9B) by using a special magnetic cap structure based on ultrathin multilayers of $[Co/Pt(Pd)]_N$. This specific composition exhibits perpendicular magnetic anisotropy (magnetic moment points perpendicular to the sample surface), even when deposited on arrays of spherical particles with sizes ranging from 50 nm to 5 μm.[121] The application of a small

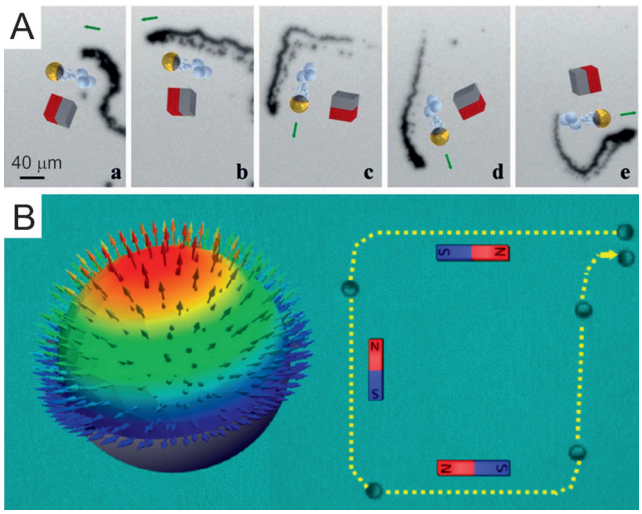

Figure 9. Magnetic control of self-propelled Janus particles. A) Time-lapse micrographs showing the magnetic control of a Mg Janus micromotor in seawater. B) Left: Distribution of magnetic moments in the cap of a spherical catalytic Janus particle coated with $[Co/Pt(Pd)]_N$. Right: magnetic control of the motion of a Janus micromotor. Reprinted from Ref. [93] (A) and Ref. [73] (B) with permission.

external magnetic field below 10 Oe can reorient the direction of motion along the *x*- or *y*-axis, which is illustrated by the square-like trajectory in the inset of Figure 9B. Moreover, the magnetically controlled Janus micromotors can not only change their direction, but also stop their motion on demand when the external magnetic field is reoriented between the *y*- or *z*-axis. The abilities of these singular magnetic Janus micromotors were demonstrated by employing them for manipulation, transportation, and sorting of microobjects in microfluidic channels.[73]

Tuning the shape of spherical MNMs leads to motion control through geometry. For example, the deposition of a TiO_2 arm on self-propelled particles half-coated with Pt results in rotational motion of the motor.[85a] Alternatively, the TiO_2 arm can be coated instead of the sphere with a Pt layer to obtain curved trajectories.[85b] Self-propelled spherical dimers also showed quasilinear and quasicircular trajectories, depending on the relationship between the size of the two monomers.[88]

2.2.4. Externally Actuated Spherical Motors

Besides autonomous Janus particles self-propelled by means of catalytic reactions, there are a number of studies showing examples of externally actuated Janus particles. In 2010, Jiang et al. reported the propulsion of Au-silica Janus microspheres by self-thermophoresis under laser irradiation.[122] The Au cap absorbs the laser irradiation and generates a local thermal gradient of temperature that induces motion. Qian et al. theoretically modeled the temperature gradient of a Janus particle irradiated with a laser and illustrated 3D motion of an Au-PS Janus particle experimentally.[123]

In 2011, Loget and Kuhn proved the linear motion of conductive Janus spheres induced by bipolar electrochemistry (BPE).[7b] The fundamental idea of BPE is based on the fact that when a conducting object is placed in an aqueous solution in which an external electric field is applied between two electrodes, a maximum polarization voltage ΔV occurs between the two hemispheres of the object.[124] The value of ΔV is given by Equation (4). Here, E is the electric field and l is the characteristic dimension of the object.

$$\Delta V = El \tag{4}$$

When the ΔV value is appropriate, redox reactions are successfully achieved at the opposite poles of the particle. For example, asymmetric bubble propulsion as a result of water electrolysis can result in translational motion.[7b] Additionally, the bubble propulsion speed can be enhanced by adding to the solution sacrificial compounds which are easier to oxidize or to reduce than H_2O molecules, and leads to bubble formation only in one of the hemispheres of the Janus motor. In 2014, Wu et al. demonstrated the propulsion of Pt-PS dimers under an electric field.[125]

Bechinger and co-workers illustrated light-actuated Janus micromotors in critical mixtures of water and 2,6-lutidine.[126] Janus micromotors were prepared by depositing a Au layer on one of the hemispheres of paramagnetic silica particles, and functionalizing the Au surface with carboxylic thiols to obtain hydrophilic caps. When the Janus micromotors were irradiated by external light ($\lambda = 532$ nm), the authors observed ballistic trajectories of the Janus particles. The swimming mechanism was addressed in a separate study,[127] which concluded that the illumination of the Janus micromotors produces a local asymmetric demixing of a critical binary mixture that generates a concentration gradient around the particle, thereby producing locomotion by a self-diffusiophoretic mechanism.

In 2013, Baker et al. described a polymeric microsphere motor that initiates the pumping of surrounding fluid when the microsphere is exposed to UV light, and is capable of keeping pumping even after the UV light has been removed.[128] The ability of the micromotor to continue performing its function is caused by a self-propagating autoinductive reaction involving reagents which are grafted onto the polymeric material of the microsphere motor.

2.3. Tubular Micro- and Nanomotors

Tubular microjets have multifunctional architectures that allow the systems to contain biological moieties on the interior and/or exterior. The bubble propulsion mechanism overcomes the limitation of the self-diffusiophoretic mechanism, so that motion in high ionic media and in biological fluids is possible.

2.3.1. Fabrication of Microtubular Motors

Microtube-based micromotors (or microjet engines) were pioneered by Mei et al. in 2008.[133] Those architectures were based on the rolling up of pre-stressed thin nanomembranes,[134] thereby enabling the fabrication of tubular structures in a deterministic manner, and showing an exceptional versatility in terms of the design and composition of the materials. In principle, any type of substrate on which photolithography can be performed (Figure 10A) is suitable for this technique. After patterning of the sacrificial layer, the thin films are evaporated at a tilted angle to generate a shadow window where no material is deposited. This window provides a gap for guiding the selective etching of the sacrificial layer. The rolling up principle consists of the difference in the internal strain between the first deposited layer containing compressive strain (yellow, Figure 10B) and the upper layer with tensile strain (blue, Figure 10B). Etching of the sacrificial layer releases the multilayer and allows lattice rearrangements, whereby the upper layer shrinks and the lower layer expands (Figure 10B). Microtubes with diameters from 1 μm to about 30 μm can be fabricated by tuning parameters such as the deposition angle, thickness, and temperature.[132] Multiple layers can constitute the rolled-up microtubes, as shown in Figure 10C, and other sacrificial layers can also be utilized to form compact tubular devices that enable diverse functionalities to be integrated in a single microtube.[135] The use of water-soluble sacrificial layers will provide future directions, such as the functionalization of microtubes with biomolecules or micropatterning of the structure.[136] Moreover, oxides and polymers can be rolled-

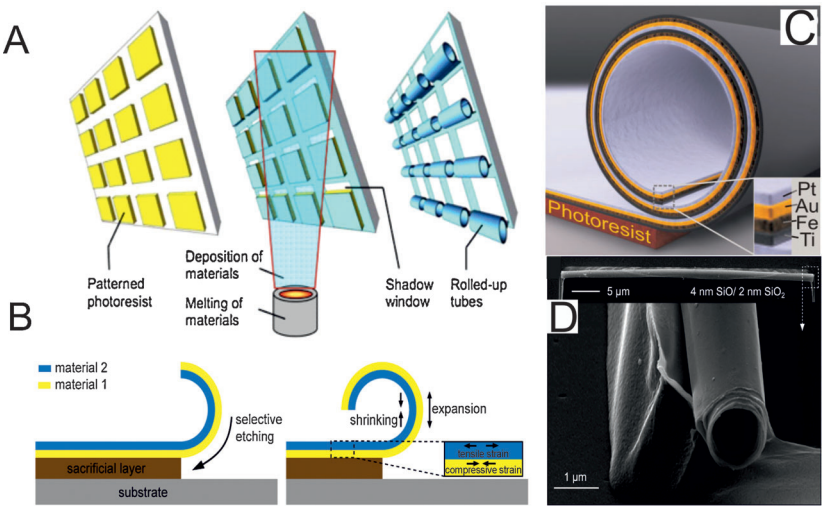

Figure 10. Rolling-up of nanomembranes to form microtubes. A) Substrate is patterned with sacrificial layers, followed by evaporation of metals at a glanced angle, which creates a window for deterministic rolling. B) Rolling up of bilayers. C) Schematic representation of a multilayer microtube. D) Oxide microtube anchored to the substrate. Reprinted from Ref. [129] (A), Ref. [130] (B), Ref. [131] (C), and Ref. [132] (D) with permission.

up by engineering the strain[132,137] (Figure 10D), and more complex 3D structures consisting of metal polymers have recently been reported.[138]

2.3.1.1. *From Tubes to Catalytic Motors*

When catalytic materials such as Pt or Ag are deposited as the top layers (Figure 10C), they constitute the inner wall of the microtubular motors. Several configurations have been reported: Ti/Fe/Au/Ag,[133] Ti/Fe/Au/Pt,[131] SiO/SiO_2/Au-catalase,[132] Ti/Au-catalase,[24] Ti/Cr/Pt,[139] Ti/Fe/Pt,[140] and Fe/Pt,[141] where Ti is used for enhanced adhesion to the sacrificial layer, Fe (or Ni) for magnetic guidance, Au for enhanced adhesion of the catalytic layer and for biofunctionalization, Cr provides improved strain for rolling, and SiO_x provides transparency, is optically active, and can be functionalized with silanes.

2.3.1.2. *Going Nano*

The heteroepitaxial growth of strained semiconductor layers by molecular beam epitaxy (MBE) enables the fabrication of smaller tubular structures as nanojet engines (Figure 11A),[142,143] with a smallest diameter of 280 nm obtained when a thin Pt layer (0.5 nm) is deposited on InGaAs (3 nm)/GaAs (3 nm) layers (Figure 11B). Unlike the deterministic rolling of microtubes presented above, Solovev et al. and Sanchez et al. did not pattern the AlAs sacrificial layer but covered the entire substrate.[142,143] Consequently, after manually scratching the films, the shape and size of the rolled-up nanojets was not fully controlled, thereby leading to a variety of geometries in terms of lengths and diameters. MNMs presenting different degrees of sharp edges (Figure 11C(b,c)) and also in cylinder form (Figure 11Ca) were obtained.[143]

Despite the excellent versatility of the roll-up nanotechnology, expensive facilities such as clean rooms and evaporators are required. The Pumera research group reported two simplified alternatives for producing rolled-up microtubes in a fast and scalable fashion at extremely low cost.[144] The authors used transmission electron microscopy (TEM) grids as masks and a small magnetron sputtering machine for the deposition of thin metallic films.

In a first process, poly(metyl methacrylate) (PMMA) was employed as a sacrificial layer, which was followed by Pt sputtering and ultrasonication (Figure 12A). Although the size of the tubes was in principle determined by the TEM grid (60 μm^2), a distribution from 20 to 60 μm in length was observed. In a second process, the TEM grid was directly placed on the glass substrate followed by Pt deposition (Figure 12B). After removing the grid, the tubes were exposed to H_2O_2. The bubbles generated at the edges of the film delaminated the Pt films, causing them to roll up into microtubes of 20 μm average length.

Yao et al. demonstrated the spontaneous rolling of multilayered structures based on graphene oxide (GO) nanosheets, Ti, and Pt.[145] After drop-casting of an aqueous solution of GO on a Si wafer, electron-beam evaporation of Ti/Pt was carried out. Figure 12C shows an SEM image of thin films

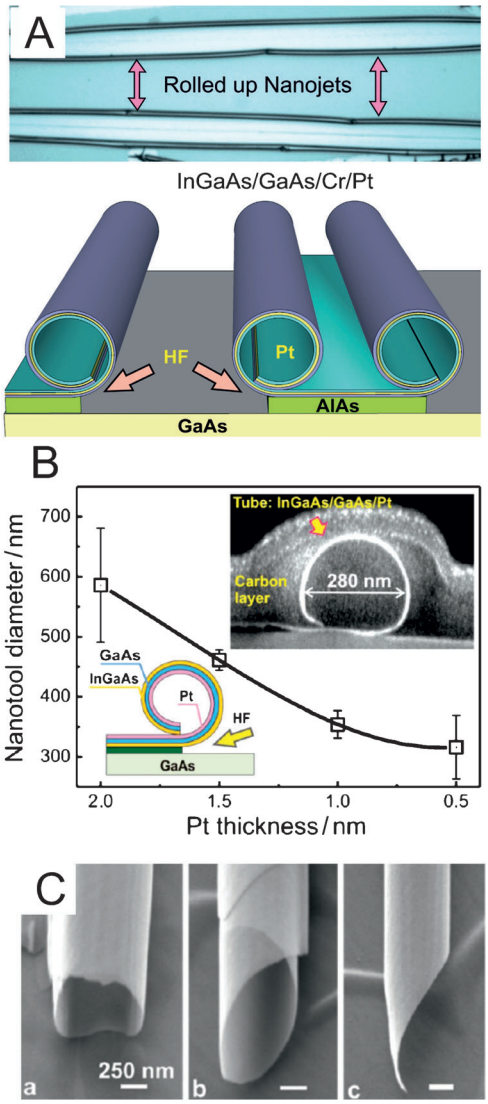

Figure 11. Roll-up of nanotubes by heteroepitaxial growth. A) Optical image and schematic representation of a scratched film leading to a double tube. B) Scalability of nanojets. C) Different types of edges found in rolled-up nanojets. Reprinted from Ref. [142] (A) and Ref. [143] (B,C) with permission.

before and after deposition of Ti/Pt. Upon sonication, the GO/Ti/Pt layers roll-up into microtubes with diameters of 1–2 μm and lengths of 10–20 μm (Figure 12C, right panel).

Li et al. took advantage of the surface tension of metal droplets deposited on strained nanofilms to produce self-rolled tubes with diameters in the range of hundreds of nanometers.[146] The top metallic layers were coated with metallic nanoparticles (Au, Ag, or Pt) and then annealed at 500 °C for short periods (10–30 s). The surface tension forces the oxide layers to roll up into tight and small tubes (Figure 13A). The layers were released from the substrate when the PMMA sacrificial layer was removed during the annealing process. A mechanical model to explain the fabrication of the nanoparticle-assisted rolling process was elaborated.[146] The results show that the particle-assisted rolling up of 6 nm membranes is about 7 times smaller than

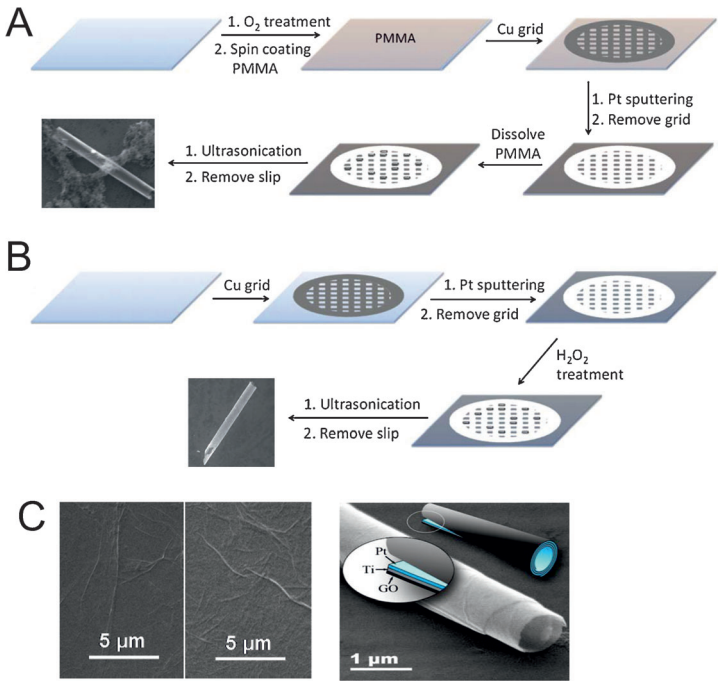

Figure 12. Fabrication of roll-up microtubes without the need for a clean room. A,B) Cheap and fast methods using TEM grids for patterning the structures. C) Roll-up scrolls with graphene oxide as an external layer. Reprinted from Ref. [144] (A,B) and Ref. [145] (C) with permission.

rolled-up microtubes based only on strain engineering without particle coating (Figure 13B). The catalytic microjets prepared by this method present higher velocities (about 195 bdl s^{-1}) than those fabricated using smooth Pt films.

The same research group reported a method that combines strain engineering and template fabrication.[147] Metals were evaporated onto porous AAO membranes which were dissolved in alkali media (Figure 13C). The presence of nanopores provided a high order of geometric complexity and the large surface area to volume ratio enabled catalytic microengines to be developed that move faster than those with smooth walls. Mechanical scratching (10–30 μm quadratic shapes) was applied to the samples, thereby resulting in tubes of variable sizes from 10–40 μm in length and 4–10 μm in diameter.

Electroplating allows the simplified mass production of catalytic microtubes. This technique requires inexpensive equipment, that is, potentiostat/galvanostat, and commercially available microporous membranes. This method does not require a clean room and costly metal evaporators, and moreover rapidly produces microtubes (see Section 2.1.1).

The Wang and Pumera research groups combined electroplating methods widely utilized in the fabrication of nanowire-based MNMs with the bubble-propelled performance of tubular microjets (Figure 14A,C respectively).[148] Two geometries can be obtained (cylindrical or conical), entirely depending on the geometry and type of porous template (either PC or AAO). In addition to many metals, the combination of polyaniline (PANI), polypyrrole (PPy), or poly(3,4-ethylenedioxythiophene (PEDOT) polymers with Pt produces catalytic microjets.[149] Moreover, the wall can be tailored with molecularly imprinted polymers (MIPs) so that selective recognition cavities can be implemented for the selective isolation of biomolecules.[150] The electrodeposition of an inner layer of Zn produced microjets that were able to be propelled by H_2 bubbles in acidic media.[151]

Zhao and Pumera successfully produced concentric bimetallic microjets and nanojets by the electrodeposition of Cu/Pt on AAO.[152] The deposition parameters were tuned so that the metals were deposited on the walls and do not fill the porous cavities.

2.3.2. *Bubble Propulsion Mechanism*

The tubular structures described in the previous section contain active materials as the inner wall for the decomposition of chemicals into gas molecules. Those materials can be catalytic or noncatalytic and decompose diverse fuels, although the main fuel that has been considered so far is H_2O_2.

The motion of microjets is described in three stages: First, the fuel solution wets the catalytic material containing energetically favorable nucleation points, where the O_2 accumulates and grows as bubbles (Figure 15A). In a second stage, the bubbles migrate towards one opening of the microtube—normally the larger opening—and finally, the bubbles are released, thereby inducing another motion step. The stepwise motion was described in several reports (Figure 15B).[131,133,153] Solovev et al. determined that the velocity of the microjets was linear to the product of the bubble radius and the frequency, with the deviations at large values attributed to the potential collisions between bubbles, which diminishes the distance travelled from the bubbles inside the tube and limits the releasing stage. The dynamics of microjets is affected by the geometry, viscosity of the medium, and the fuel composition.

2.3.2.1. *Geometry Constraints*

If the microjet is a symmetric cylinder, bubbles are released in a linear manner, which is translated into a linear motion. If the edges are not flat (see Figure 11C), bubbles leave the microjet at an angle, thereby inducing a torque so that circular, spiral, or curved trajectories are observed (Figure 15C).[131,143]

2.3.2.2. *Viscosity and Medium*

MNMs move at low Re values, where inertia is negligible and viscous forces are dominant. Sanchez et al. reported the superfast motion of microjets at physiological temperatures, where viscosity is reduced by 50%. Under those conditions, the dynamics of the microjets varied from linear to circular motion.[139] Reducing the viscosity of the media enabled microjets to move in reconstituted blood samples at physiological temperature,[141b] with the motion hampered at 25°C.[154] Pumera and co-workers studied the motion of microjets at different Re values, and concluded that circular

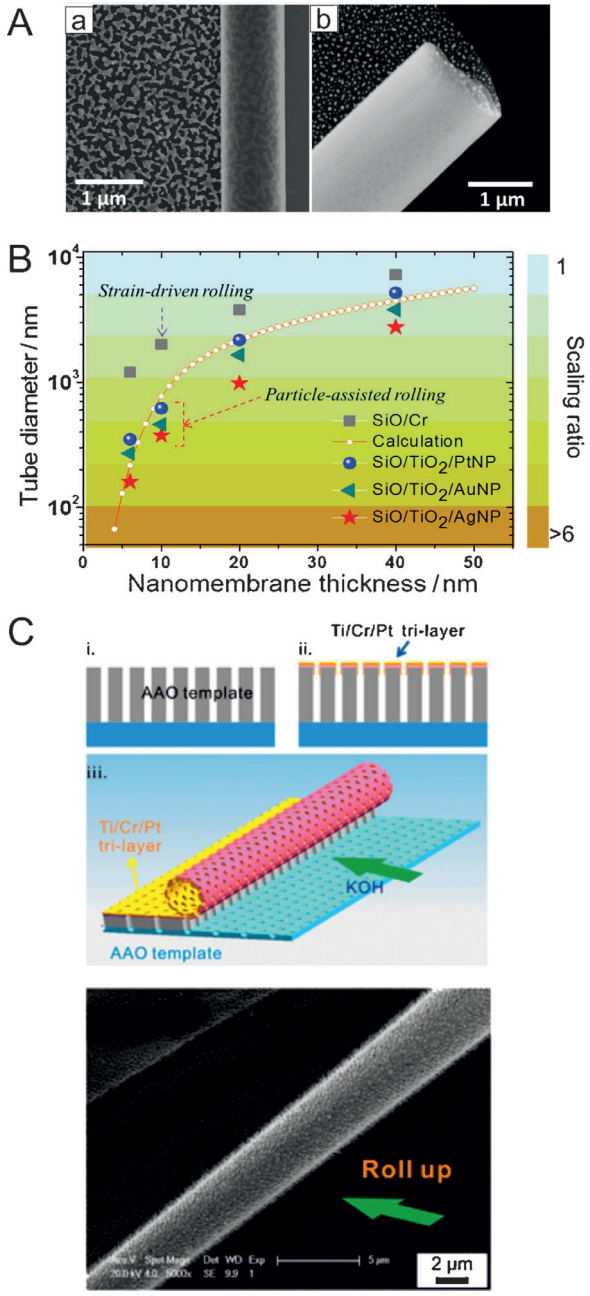

Figure 13. Rolling up of nanofilms by variable methods. A,B) Particle-assisted rolling. C) Template-based roll-up of strained nanomembranes. Reprinted from Ref. [146] (A,B) and Ref. [147] (C) with permission.

motions (or nonlinear) are preferable at higher Re values,[155] in agreement with the findings by Sanchez et al.[139]

The components of the solution can sometimes dramatically alter the swimming performance of microjets. Blood metabolites,[156] proteins,[157] extracellular thiols,[158] electrolytes,[159] and also sources of water may affect the motion of microjets.[160]

2.3.2.3. *Fuel Composition*

Both components of the fuel, that is, H_2O_2 and surfactant, determine the motion of the microjets. Speed normally

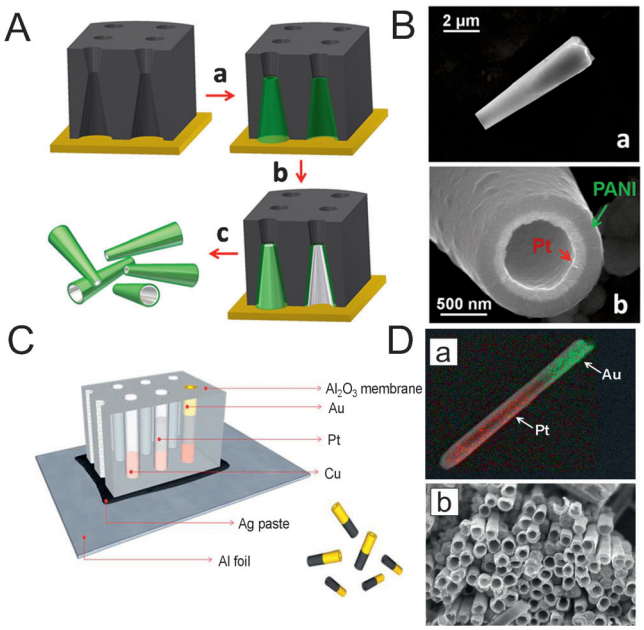

Figure 14. Template-based fabrication of tubular microjets. A, B) Schematic and SEM images of onical microjets using a PC template. C, D) Schematic and SEM images of bimetallic concentric micro- and nanojets using AAO membranes. Reprinted from Ref. [148b] (A,B) and Ref. [148a] (C) with permission.

increases as the H_2O_2 concentration increases, reaching a plateau at high concentrations, similar to the Langmuir adsorption isotherm or the Michaelis–Menten Equation for enzymatic reactions. The addition of surfactants to the fuel solution not only aids the contact of the fuel with the catalytic inner layer but also stabilizes the generated microbubbles and ensures their continuous release.

For that purpose, a large variety of surfactants have been used so far, that is, common soap, benzalkonium chloride (BCl), sodium cholate, triton-X, sodium dodecyl sulfate (SDS; for a summary see Ref. [161] and references therein). It was not until this year, however, that the Pumera and Sanchez research groups systematically studied the influence of several surfactants (cationic, anionic, and non-ionic) on the motion of microjets.[106,161] The velocity of the microjets is enhanced on increasing the concentration of an anionic surfactant below the critical micelle concentration. Cationic surfactants result in either a reduction in the speed at high concentrations or no mobility at all. Non-ionic surfactants show a more constant effect or a slow increase in the speed. The main difference in the mobility of the microjets is attributed to the adsorption of surfactants onto the inner catalytic layer.[106,161]

Interestingly, Simmchen et al.[106] and Zhao and co-workers[145] observed that microjets can also self-propel without the use of surfactants at 10 and 5 wt% H_2O_2, respectively. Nonetheless, those H_2O_2 concentrations are about one order of magnitude larger than if surfactants are added to the fuel solution.

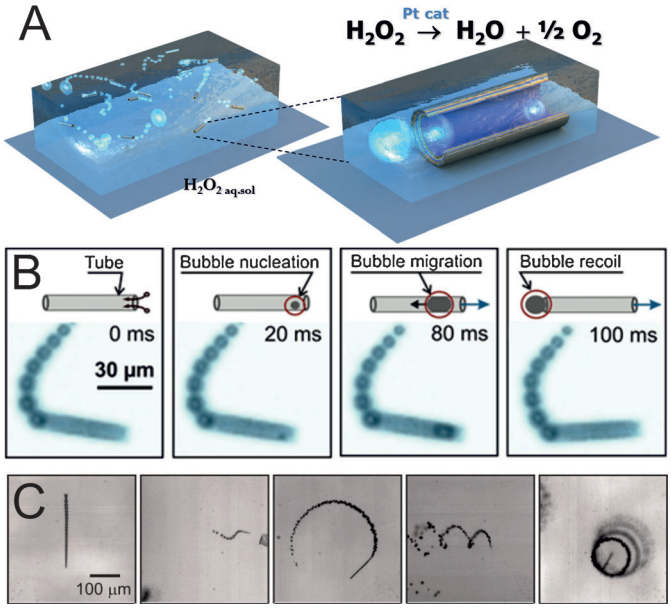

Figure 15. Bubble-propelled microjets. A) Schematic representation of multiple microjets self-propelled by bubble generation and release. B) Stepwise mechanism of motion. C) Different dynamics by asymmetric bubble release. Reprinted from Ref. [153a] (B) and Ref. [131] (C) with permission.

2.3.2.4. *Theoretical Models*

Manjare et al. described that bubble growth and ejection cause the microjet to move.[162] Their model investigates the effects of geometrical parameters such as microjet length and opening diameter on the mass transport of H_2O_2 and O_2 across the microjet. However, they only considered that bubbles grow at the end of the tubes and did not consider the migration step, which was previously observed to contribute to the motion. The authors used the same mechanisms described previously by the same research group, thus imposing a growth force governed by the Rayleigh–Plesset Equation.[113]

A model reported by Li et al. together with experimental results was based on a system where the bubbles and tubes are considered separately.[163] The authors assumed that when the bubble and tube are at a distance of a tube diameter, both stop at the same time. This system is controversial since after separation, the dynamics of the bubble and tube may be different and not necessarily correlated. A later study by Fomin et al. combined experimental results with a theoretical model based on the time-dependent hydrodynamic analysis of the formation and migration of a growing bubble in an asymmetric microtube. This migration leads to a capillary force that produces a jet effect which propels the tubes.[164] The model was compared with the other two proposed models and provided complementary key parameters, such as the motion of bubbles inside microtubes and a related momentum transfer. It was hypothesized that asymmetries other than geometrical could give rise to motion mechanisms in perfectly symmetric tubes, as observed experimentally. Recently, Li et al. introduced a theoretical model combined with experimental results to describe the hydrodynamics of self-propelled conical microtubes and the forces acting on the microtube and the bubble during bubble growth at the end of the microtube before ejection of the bubble.[165] Their model considers both the bubble geometry and buoyancy force. More developed models would help to understand all the motion steps observed experimentally.

2.3.3. *Motion Control of Microjets*

2.3.3.1. *Magnetic*

When a ferromagnetic layer (Fe) is integrated into the tubular structure, microjets align according to the direction of the magnetic field.[153a] Solovev et al. localized microjets containing magnetic material in circular motions when a rotating magnetic field was applied to the sample.[131] The guidance of microjets was reported soon after by using a permanent NdFeB magnet to produce a field of 50 G around the sample. The external control allows their use as carriers and for targeted delivery, as will be covered in Section 3.1. These methods, although effective on their own, lack precise control and control over single motors.

The individual control of microjets in a closed-loop manner and 3D motion control were the next steps to be taken. Recently, collaboration between the Sanchez and Misra research groups led to a series of publications on the accurate closed-loop control of microjets.[166] The authors demonstrated precise point-to-point closed-loop control by using weak magnetic fields (2 mT).[166c] Another study demonstrated precise control when a flow was applied against and along the direction of the microjets.[166b] An electromagnetic system consisting of two sets of orthogonal arrays of electromagnetic coils with an iron core in conjunction with two microscopic systems was used to control the motion of microjets in 3D space (Figure 16A).[167] Microjets overcome vertical forces, such as buoyancy forces, interaction forces with O_2 bubbles, and vertical flow, so that they are capable of diving downwards and swimming upwards relative to reference positions.

2.3.3.2. *Temperature*

The temperature of the solution can be controlled by two Peltier elements in connection with a dc power supply placed underneath the sample containing microjets.[139] By heating the system to a physiological temperature, microjets increase their efficiency and are propelled at very low concentrations of H_2O_2 (140 $\mu m\,s^{-1}$ at 0.25%; Figure 16B, micrographs). Furthermore, at 5% H_2O_2, the microjets reach record speeds of 10 $mm\,s^{-1}$. The toxicity of the fuel was tested by using a MTT (3-(4,5-dimethylthiazol-2-yl)-2,5-diphenyltetrazolium bromide) viability assay for fibroblast NIH-3T3 cells. The results showed that only 40% of the cells were viable after 1 h of treatment with the lowest concentration of H_2O_2 capable of propelling microjets (i.e. 0.25%). For a more cell-friendly environment, the H_2O_2 concentration needs to be reduced further to prolong micromotor–cell interactions. The same setup was used to activate microjets in blood samples.[141b] At 25 °C, microjets were not propelled in 10 times diluted red blood cells (RBC). Motion was also not observed in a 10 times

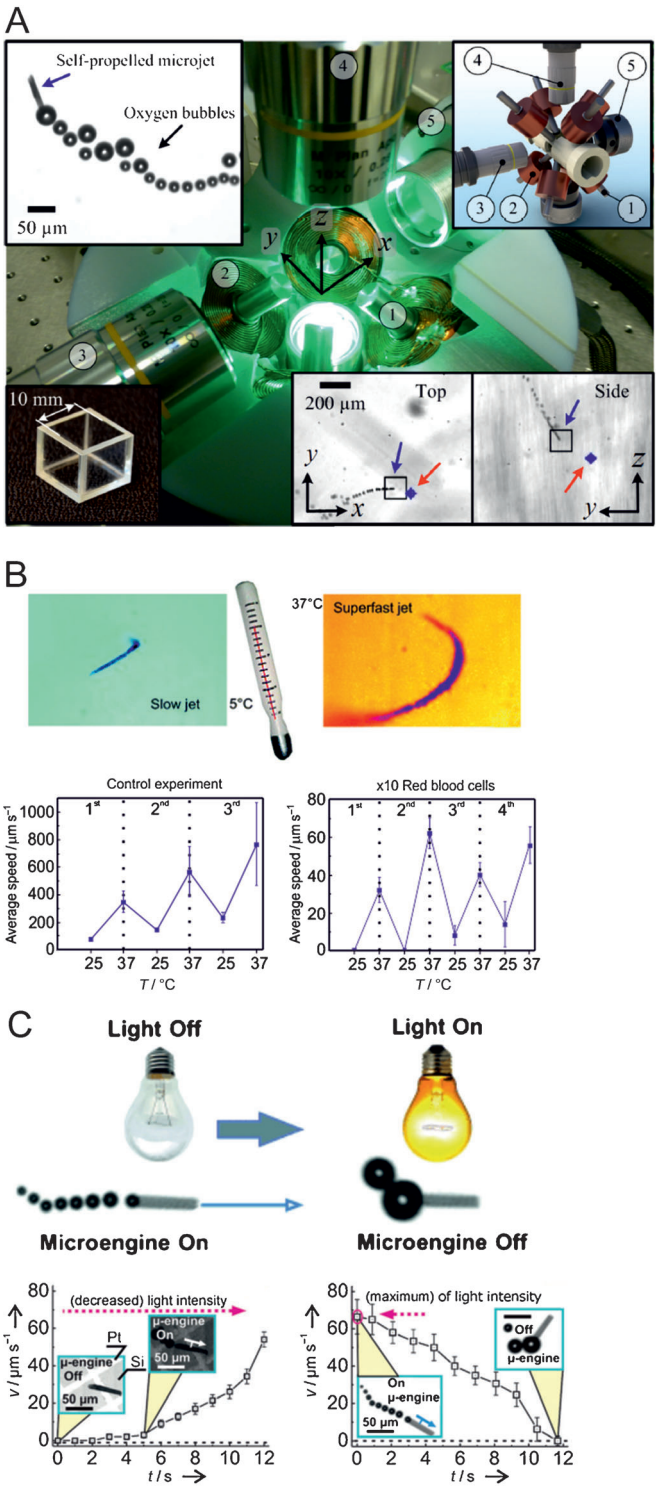

Figure 16. Methods for the remote control of microjets. A) Magnetic field. B) Temperature. C) light. Reprinted from Ref. [167] (A), Ref. [139, 141b] (B), and Ref. [168] (C) with permission.

concentrated RBC with 10 times concentrated serum. However, at 37 °C the viscosity of the fluid containing cells is reduced and the efficiency of the microjets increased (Figure 16B, plots). These results demonstrated the proof-of-principle of microjets in lab-on-a-chip devices in bio-analytical applications.

Soft micromotors composed of flexible thermoresponsive polymeric microjets can reversibly fold and unfold in an accurate manner in response to changes in the temperature of the solution in which they are immersed, thereby allowing them to rapidly start and stop multiple times in response to the radius of curvature.[137a] The use of stimuli-responsive materials would be ideal for future designs of smart MNMs.

2.3.3.3. *Light*

Solovev et al. demonstrated the control of microjets by using a white light source (Figure 16C).[168] This process was mediated through illumination of the fuel solution above Pt-patterned Si surfaces, which induces a local decrease in the H_2O_2 and surfactant concentration. Although white light could be used to switch off the propulsion of the microjets, shorter wavelengths were observed to suppress the generation of microbubbles faster than did longer wavelengths. The phenomenon is reversible; thus, a non-active microjet is activated by dimming the light source. The on/off process is, however, not immediate as it requires a few seconds to completely stop or to acquire a stable maximum speed.[168]

2.3.3.4. *Chemical Gradients*

Solovev et al. showed that the generation of large microbubbles from small ensembles of microjets produced a capillary force and a chemophoretic attraction force that pulled other microjets into the swarm.[11e] A more sophisticated experiment was reported by Baraban et al., who presented a controllable way of studying the chemotactic behavior of two types of MNMs—Janus motors and tubular microjets—in microfluidic channels.[11j] Both types of motors move towards the gradient of the fuel without the influence of capillary forces (Figure 17A). The chemotactic motion was found to be dependent on the concentration of the chemoattractant as well as on the size and shape of the artificial micromotors. The experimental results could lead to possible applications, such as the separation of objects on the micrometer and nanoscale or attraction to pollutants in water.

2.3.3.5. *Microchips and Physical Boundaries*

Catalytic MNMs interact with the walls surrounding them. Restrepo-Pérez et al. demonstrated the trapping of micromotors and the elimination of the need for external energy sources to control their motion.[169] The technique relies solely on steric boundaries present on microfluidic chips containing chevron and heart-shape engineered structures (Figure 17B). Chevron-shaped structures with angles from 40 to 140° were fabricated from PDMS, and showed a higher trapping efficiency than smaller angles, as previously predicted theoretically.[171] Heart-like shapes and ratchets have recently been used to sort and guide *E. coli* and sperm cells in microfluidic devices.[172]

Microjets can be concentrated in heart-like reservoirs with 40° chevron tips, thereby preventing the return of the microjets to the main reservoir, while the ratchet reduced the amount of motors escaping from the chamber. This on-chip

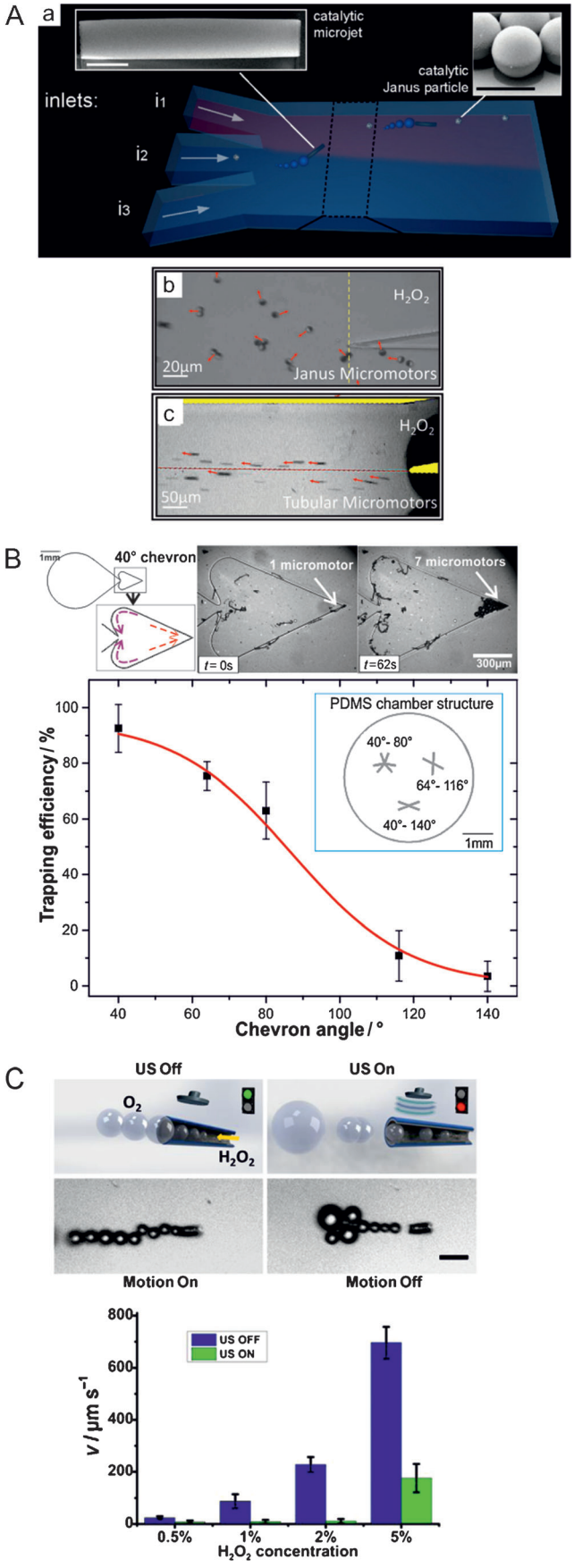

Figure 17. Methods for remote control of microjets. A) Chemical gradient. B) Microchip. C) Ultrasound. Reprinted from Ref. [11j] (A), Ref. [169] (B), and Ref. [170] (C) with permission.

concentrating system was used to trap biofunctionalized microjets for the facile integrated method for the concentration of biomolecules and the creation of portable bioanalytic devices.[173]

2.3.3.6. *Ultrasound*

The generation of bubbles can be disrupted by an ultrasound field. The Wang research group reported reversible control of the movement of PEDOT/Ni/Pt microengines by tuning the applied voltage of the external transducer which

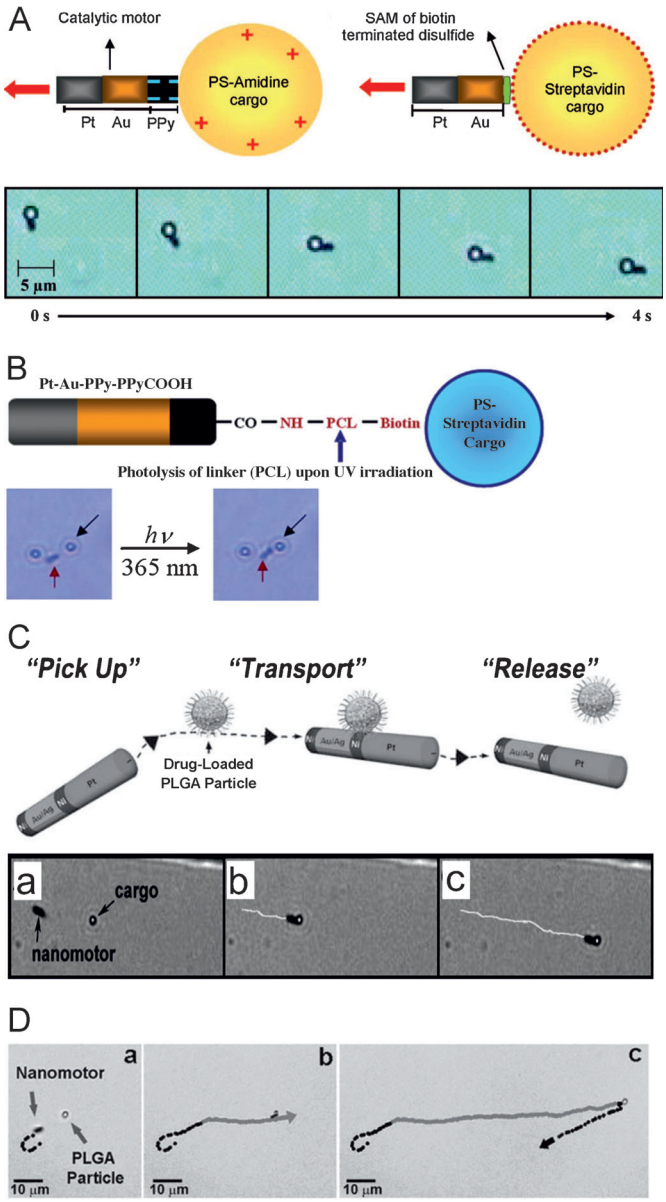

Figure 18. Transport of cargo using nanowire-based MNMs. A) Specific loading and transport by electrostatic and covalent binding of PS cargos. B) Light-induced release of cargo. C) Magnetic pick-up of microparticles and their transport in microfluidic channels. D) Release of drug-loaded particles by rotation of the magnetic field. Reprinted from Ref. [174] (A), Ref. [175] (B), Ref. [176] and Ref. [61b] (C), and Ref. [176] (D) with permission.

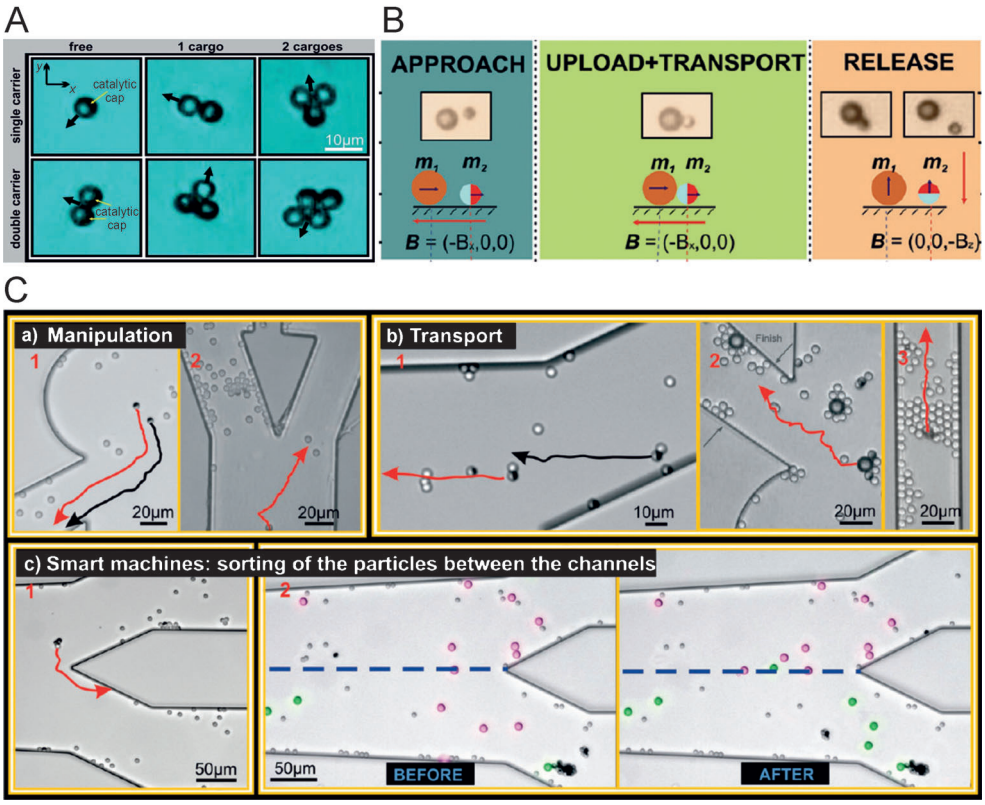

Figure 19. Transport of cargo using Janus micromotors. A) Individual and collective transport of PS particles. B) Magnetic guidance towards a large cargo, load, and release using magnetic rotation. C) Manipulation, transport, and sorting of obstacles in microfluidic channel networks. Reprinted from Ref. [100] (A) and Ref. [73] (B,C) with permission.

generates the ultrasound field. The authors reported extremely fast changes in the motor speed (< 0.1 s) and reproducible on/off activations that were faster than other reported methods for stopping the motion of microjets (Figure 17 C).[170]

3. Applications of MNMs

3.1. MNMs as Carriers/Microshuttle Actuators

Catalytic MNMs offer the ability to load, transport, and deliver cargoes at precise locations. The Sen research group demonstrated two methods for towing PS microparticles by using metallic nanowires: 1) electrostatic interaction, by attaching a positively charged PS-amidine cargo to a negatively charged PPy segment at the end of the rod; and 2) biotin–streptavidin interaction, whereby the Au end of the Pt/Au rod was functionalized with biotin and the PS was coated with streptavidin (Figure 18 A,B).[174]

Subsequent studies demonstrated the release of cargo by dissolving the Ag segment in the presence of H_2O_2, chloride ions, and UV light.[175] The process of release needed 10–20 s exposure to UV light. An improved release method consisted of the release of a photocleavable linker (PCL) through photolysis of an *o*-nitrobenzyl group contained in the linker attached to the cargo (Figure 18 B). Although this second method caused no poisoning of the motor by Ag precipitation, the time required for release is longer (60–100 s). The Wang research group took advantage of the magnetic properties of striped nanowires Pt(CNT)/Ni/Au/Ni/Au to load iron oxide encapsulated microparticles[61b] and drug-loaded liposomes into microfluidic channels (Figure 18 C.a–c).[176] The MNMs were magnetically guided and the release was achieved by rapid rotation of the external magnet by 180° (Figure 18 D).

Metallic nanowires presented two main limitations that hindered their application as transporters in biological media: their low power output to move large biological cargoes and their electrokinetic mechanism, which is not compatible with high ionic media.

Spherical Janus particles can act as specific and nonspecific carriers. Baraban et al. demonstrated the transport of PS particles by Janus motors (5 μm diameter). Janus motors could individually or collectively transport single or multiple cargoes (Figure 19 A).[100] These different possibilities give rise to various mobility configurations. The rotation of the transporters with and without cargoes is affected by geometrical misalignments and by the variation in the distribution of the reaction products near the walls. The experimental results were modeled theoretically. In a later study, Baraban et al. realized the transport of superparamagnetic cargo and magnetic guidance of Janus motors (Figure 19 B).[73] By applying an external magnetic field, the MNMs were loaded and the cargo guided and delivered to the desired locations, and microobjects sorted in complex microchannels (Figure 19 C). The release is achieved simply by manipulating the magnetic dipole–dipole interactions between the cargo and motor by changing the orientation of the external magnetic field.

Tubular microjets exhibit several advantages for the transportation of cargo compared with other geometries. The loading of multiple spherical particles, metallic plates,[153a] and cells[177] can be achieved nonselectively (Figure 20). This simple method relies on the induced pumping of fluid into the microtubular structure by the catalytic reaction to achieve self-propulsion.[153a] The accurate transport of microparticles was demonstrated in microfluidic systems (Figure 20 A.d–f).[140] As in other magnetic microtransporters, a fast rotation of the magnetic fields enables the release of the cargo. Smaller

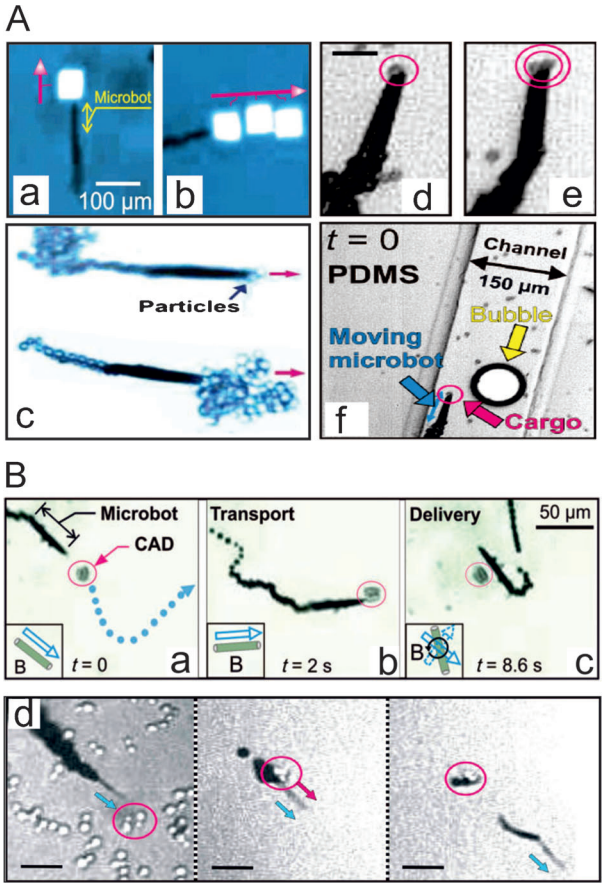

Figure 20. Nonspecific transport of cargo by tubular microjets. A) Transport of microplates (a,b; the pink arrow: indicates the direction of motion) and spherical particles (c–f) and their magnetic guidance in microfluidic channels (d–f; scale bar: 15 μm). B) Load, transport, and delivery of cells using microjets (a–c) and nanojets (d; scale bar: 20 μm). Reprinted from Ref. [153a] (A.a–c), Ref. [140] (A.d–f), Ref. [177] (B.a–c), and Ref. [143] (B.d) with permission.

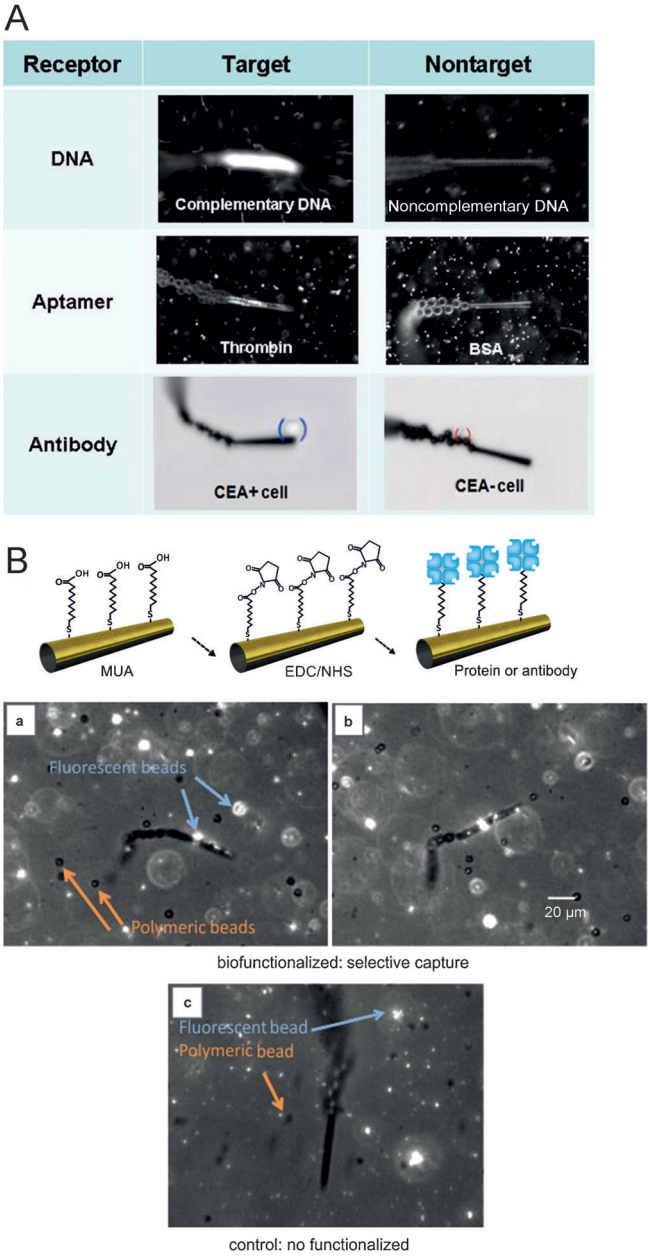

Figure 21. Selective binding and transport of biological analytes and cells by functionalized microjets. Reprinted from Ref. [179] (A) and Ref. [173] (B) with permission. CEA = carcinoembryonic antigen.

versions of catalytic jets (nanotools) have been utilized for carrying multiple yeast cells (Figure 20 B.d).[143] In this case, the cells were physically adsorbed to the outer wall of the nanojets and a fast rotation of the nanojet detaches the cells and releases them.

Magnetized rolled-up microjets can act as small self-propelled micromagnets capable of selectively picking up paramagnetic cargo in the presence of diamagnetic ones without the influence of any external magnetic field.[178]

The Wang research group demonstrated in a series of publications the great capabilities of microtubular motors for the selective capture, transport, and isolation of different target analytes of biological relevance.[179] They biofunctionalized the outer walls of microtubes with ss-DNA,[180] aptamers,[181] antibodies,[182] and lectin receptors,[183] so that the isolation of nucleic acids, cancer cells, proteins and bacteria could be demonstrated (Figure 21 A). The authors made use of roll-up microtubes with Au layers for thiol-modification and also template-assisted microjets with polymer walls.

A particularly interesting approach is the use of aptamers for the highly selective capture of thrombin, which can be released by the addition of ATP into the solution.[181] The release of bacteria is performed by dissociation of the lectin–bacteria couple by glycine at a low pH value. In a similar process, but using a poly(3-aminophenylboronic acid)/Ni/Pt conical microjet, the binding and release of yeast cells was demonstrated.[184]

3.2. Towards Biomedical Applications

Recently, Restrepo-Pérez et al. reported the selective binding of biotinilated microparticles and their concentration in defined reservoirs without the influence of an external

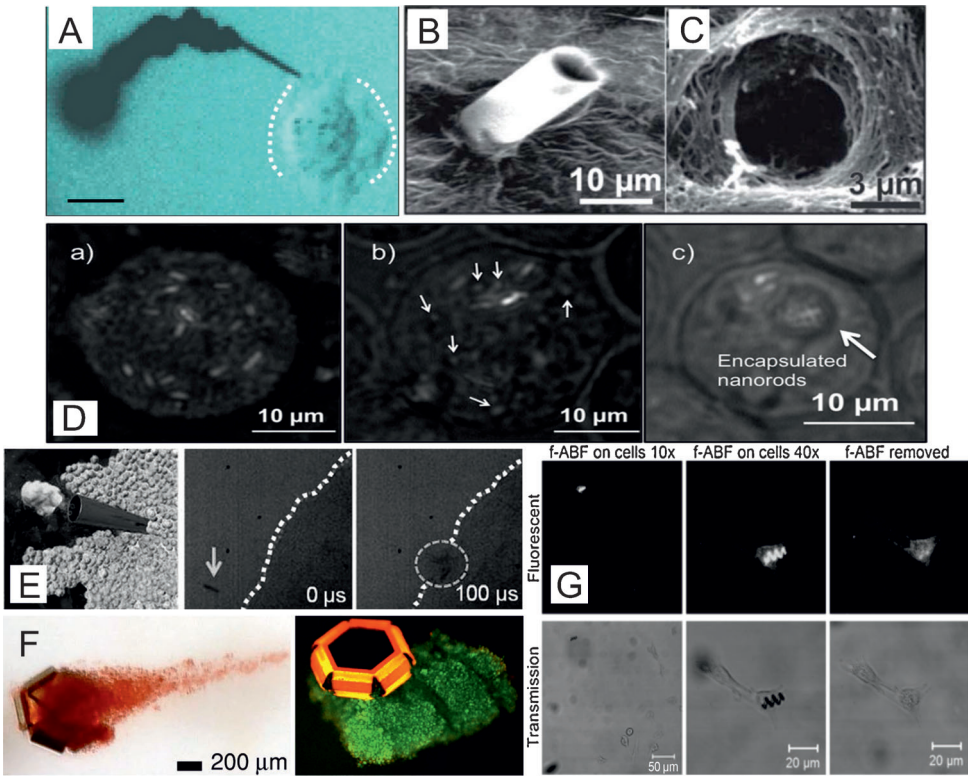

Figure 22. MNMs interacting with biomaterial such as cells and tissues. A) Catalytic nanojet drilling of a fixed cancer cell. B) SEM image of a magnetic microtube drilling into pig liver tissue, and C) hole after removing the microtube. D) Au nanorods inside living HeLa cells. a) A HeLa cell with multiple nanorods inside. b) Subcellular structures (a few are indicated by arrows) can be seen interacting with active accoustic motors inside a HeLa cell. c) Two vesicular structures in a HeLa cell containing many active but crowded accoustic motors. E) Computer-generated representation (left) and images of a microbullet penetrating a tissue after an ultrasound pulse. F) Capture of cells by thermally and biochemically triggered grippers. G) Functionalized artificial bacterial flagella delivering calcein to single cells. Reprinted from Ref. [143] (A), Ref. [188] (B,C), Ref. [9b] (D), Ref. [189] (E), Ref. [190] (F), and Ref. [191] (G) with permission.

field.[173] This study presents an alternative concentration mechanism for on-chip bioassays, where only physical boundaries play a role in the guidance of the biofunctionalized microjets (Figure 21 B).

Orozco and co-workers developed a motor-based immunoassay platform for lab-on-a-chip devices. Polymer/Ni/Pt microjets were functionalized with antibody receptors for the selective capture of proteins. This type of active on-chip sensors substitutes the standard washing steps in antibody assays.[185] The ability of bubble-propelled microjets to mix fluids[186] has been exploited in the biosensing field by Morales-Narváez et al. The authors combined micromotors with microarray technologies to improve the efficiency of the biosensing platforms by providing a continuous in situ mixing of the analytes involved in the immunoreaction.[187]

Nano- and microjets have proven capable of drilling into soft tissues and biomaterials. Rolling-up thin nanomembranes asymmetrically can lead to sharp edges being engineered. Nanojets were self-propelled and externally guided towards fixed cancer cells and embedded in their interior (Figure 22 A).[143] One limitation, however, is the toxicity of the H_2O_2 fuel needed for the propulsion, which results in the cells undergoing apoptosis after short periods. Therefore, other sources of motion are urgently needed.

Magnetic actuation can be used as an alternative to catalytic propulsion. Conical microtubes powered by an external rotating magnetic field were placed onto liver tissue and drilled into it for long periods.[188] After releasing the microtube from the biomaterial, a micrometer-sized hole was observed by SEM imaging (Figure 22 B,C). The Nelson research group developed magnetic helices that react to low external magnetic field and can act as microtransporters of cells.[4h,8b,191] The microrobots can be coated with biocompatible layers and loaded with drugs to be delivered to single cells in vitro (Figure 22 G).[191,192] The Gracias research group demonstrated that enzymatically actuated self-folding microgrippers can capture biomaterial ex vivo (Figure 22 F).[138,190]

Ultrasonic waves can also induce the motion of MNMs (Figure 22 D,E).[9a,189] Biofunctionalized nanowires moved by ultrasound have been used for biosensing[9c] and the first results of magnetic guidance towards cells have been reported.[193] Mallouk and co-workers reported the internalization of a nanowire-based motor inside living cells (Figure 22 D).[9b] Finding biocompatible fuels and materials for catalytic MNMs or the use of non-invasive external actuated MNMs may pave the way for biomedical applications of MNMs in the near future.

Recently, Sen and co-workers made use of active particles which are propelled by ion gradients for the detection of bone cracks in vitro. Particles can not only detect but also transport and deliver drugs to the crack location by using the diffusiophoretic mechanism of motion.[194] The latest advances in using MNMs for biomedical applications and drug delivery have recently been reviewed.[195]

3.3. Chemically Self-Powered Pumps

Controlling fluid flow at the microscale is a challenge in the field of MNMs. Particular attention has been given to pumps that can precisely modulate the flow rate without any external source of power. An ideal pump should also be able to respond to the presence and concentration of a specific analyte, therefore giving precise spatial and temporal control over the flow rate. Micropumps in MNMs are based on the

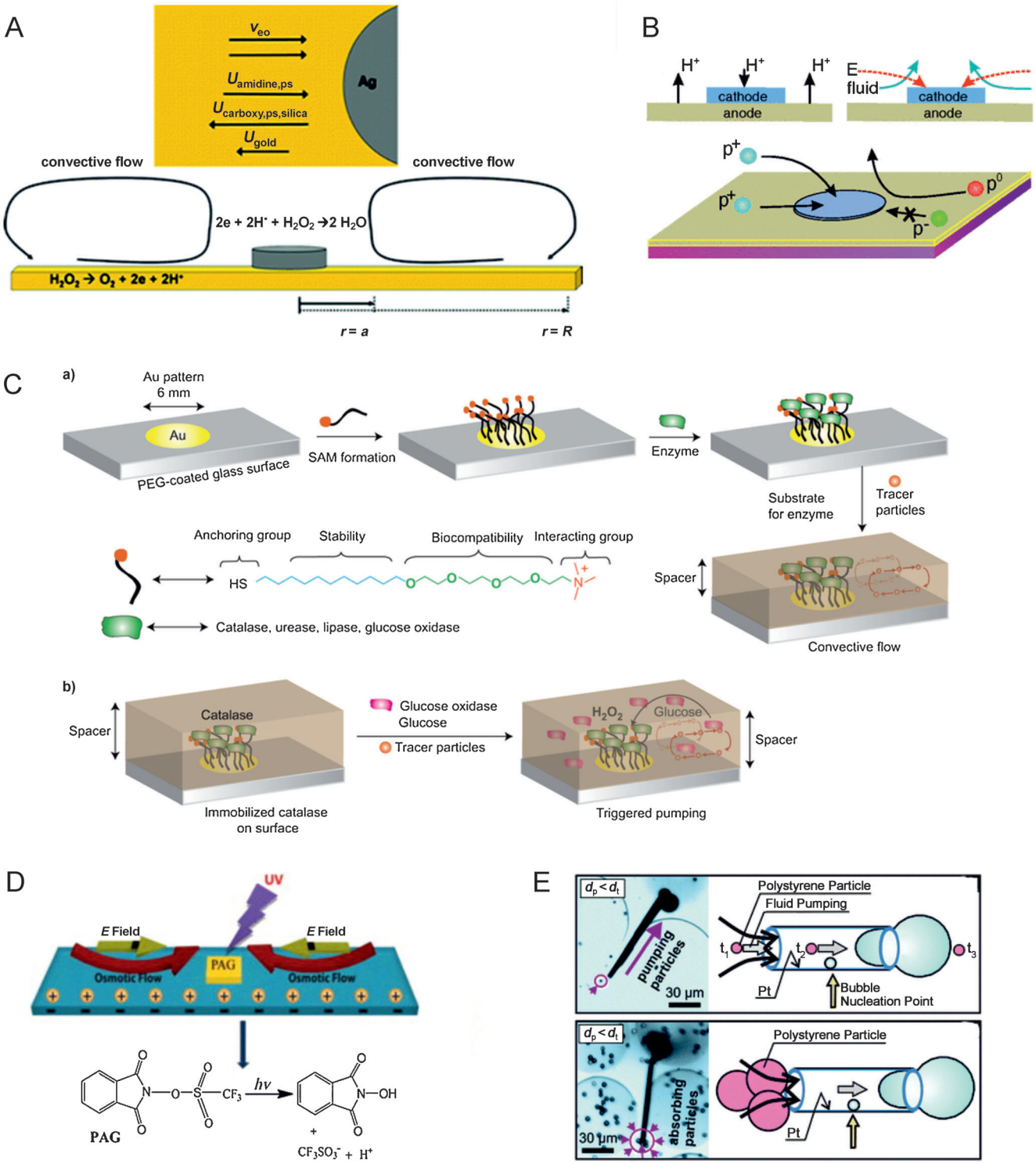

Figure 23. A) Oxidation of H_2O_2 at the Au surface creates H^+, which migrates from Au to the Ag, thereby generating an electroosmotic flow. B) The direction of the electric field and fluid flow around the Au/Pt micropump was detected using charged polystyrene spheres. C) Fabrication of enzyme micropumps as well as GOx- and glucose-triggered pumping. D) Light-triggered PAG pumping mechanism. E) Catalytic pumping of polystyrene spheres by rolled-up microtubes. Reprinted from Ref. [196] (A), Ref. [197] (B), Ref. [40] (C), Ref. [198] (D), and Ref. [199] (E) with permission.

idea that the same forces that generate the propulsion forces in micromotors can be harvested to generate flows in the fluid surrounding immobilized motors through the principle of Galilean invariance.

Sen and co-workers demonstrated flow-induced patterns in a dilute H_2O_2 solution above a Au surface that was patterned with Ag circles and rings to act as the cathode (Figure 23 A). They used carboxylated polystyrene spheres as

tracers to track the fluid flow above the catalytic surface.[196] Several systems have subsequently been developed using hydrazine as the source of power on a Au/Pd surface,[58] for example, pumps consisting of insoluble polymer films that depolymerize to release soluble monomeric products when exposed to a specific analyte,[200] as well as electrodes deposited on the opposing surface of a membrane and short-circuited to cause an ionic current which in turn creates a flow.[201] Sen and co-workers also reported pumps which could be turned on/off by external UV light[198] (Figure 23 D) and most recently enzyme-powered micropumps that used catalase, urease, lipase, and GOx to generate fluid flows (Figure 23 C).[40] Bachtold and co-workers tracked the motion of neutral, positive, and negatively charged particles near a Pt/Au pump to estimate the direction and magnitude of the electric field and fluid flow around the pump. They further used a fluorescent dye to image the H^+ gradient around the Pt/Au system and found it to agree with the observed direction of the electric field (pointing from Au to Pt) and fluid flow (Au to Pt and then upwards; Figure 23 B).[197]

Solovev et al. used immobilized tubular microjets to act as micropumps. These microtubes had an inner Pt layer which decomposed H_2O_2 into H_2O and O_2 microbubbles. They could be activated at H_2O_2 concentrations as low as 0.0009 % (v/v). By using polystyrene spheres as tracers they demonstrated that the flow of the pumped liquid matched with the growth

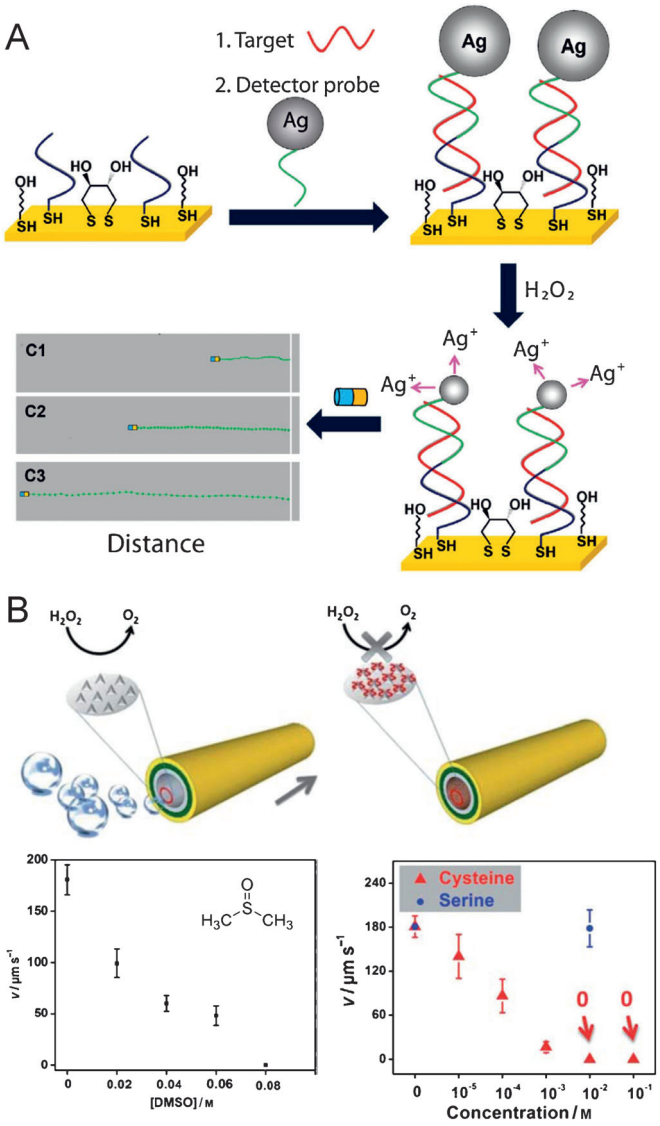

Figure 24. Application of MNMs as chemical sensors. A) Detection of Ag-tagged nucleic acid, which alters the motion of the catalytic nanowire motors. B) Effect of the concentration of DMSO, cysteine, and serine on the swimming speeds of the microtubular motors. Reprinted from Ref. [202] (A) and Ref. [158] (B) with permission.

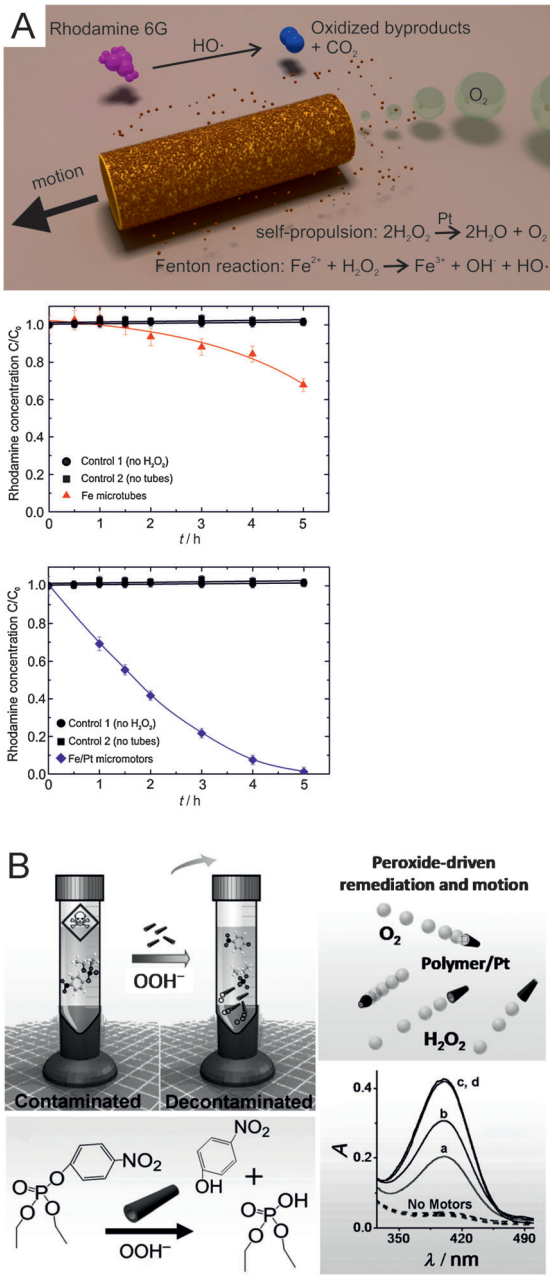

Figure 25. Remediation systems using micromotors. A) Degradation of organic pollutants by employing multifunctional Fe/Pt micromotors in H_2O_2 solutions. B) Accelerated oxidation of organophospate nerve agents by H_2O_2 by using micromotors as active mixers. Reprinted from Ref. [141a] (A) and Ref. [186b] (B) with permission.

Table 2: Potential environmental applications of MNMs.

Type of MNM[a]	Propulsion	Size [μm][b]	Max. speed [$\mu m\,s^{-1}$]	Strengths/weaknesses	Ref.
Ag-capped NPs	N/A	0.15 Ø	n.a.	-removal of pathogens, organic compounds or heavy metals. -lack of self-propulsion	[203]
MT	enzymatic	8 L 2-1.2 Ø	54	-sensing of enzyme inhibitors -nonselective response	[34]
Cu/Pt MT Ti/Fe/Cr/Pt MT	catalytic	7 L or 50 L	180	-sensing of DMSO, amino acids, and some peptides -nonselective response	[158]
Cu/Pt MT	catalytic	7 L 1.5–2 Ø	365	-increasing amount of inorganic ions caused a decrease of the micromotor speed	[160a]
PEDOT/Pt MT	catalytic	8 L	980	-increasing amount of inorganic ions caused a decrease of the micromotor speed	[160b]
Sf-PSF	Marangoni effect	mm sized	8–15 $cm\,s^{-1}$	-ability to shepherd oil droplets and merge them -unable to remove them	[204]
SAM-Au/Ni/PEDOT/Pt MT	catalytic	8 L 2 Ø	105	-capture of oil droplets -unable to release them	[205]
SAM-Au/Ni/Ti-Mg JP	redox	30 Ø	90	-capture of oil droplets -short life-time	[93]
Fe/Pt MT	catalytic	500 L 40 Ø	538	-double functionality of micromotors: water remediation + mixing.	[141a]
PEDOT/Pt MT	catalytic	8 L	n.a.	-acceleration of the oxidation of chemical threats	[186b]

[a] MT = microtube. n.a. = not available. Sf-PSF = surfactant-loaded polysulfone capsule. JP = Janus particle. [b] Ø = diameter. *L* = length.

and migration of bubbles that displaces the fluid within the tube (Figure 23 E). Different dimensions of these pumps were studied, and longer tubes were found to require lower concentrations of H_2O_2 to start pumping.[199]

3.4. Chemical Sensors

The use of MNMs as chemical sensors is based on the fact that the swimming speed of MNMs can be transformed into an analytically useful signal. The interaction of certain compounds in the sample with the catalytic sites of the MNMs is evaluated from the alteration of their swimming speed and is related to the concentration of an analyte in solution (Figure 24). Although the field is still in its infancy, the use of MNMs for chemical sensing may have a number of advantages over conventional electrochemical or optical sensors, such as selectivity, sensitivity, immunity to electrical interferences, operation in a wireless manner, and only requiring a minute amount of sample. In the last five years, several research groups reported the capability of MNMs to detect heavy metals,[34,64,206] inorganic electrolytes present in blood,[159] organic compounds such as dimethyl sulfoxide (Figure 24 B),[158] uric acid,[156] blood proteins such as bovine serum albumin (BSA), γ-globulin, and glucose oxidase enzymes,[157] amino acids containing thiol groups, for example, cysteine, serine, and methionine (Figure 24 B), peptides such as glutathione,[158] and DNA (Figure 24 A).[202]

Catalytic MNMs can also be employed as pH sensors, by exploiting their pH taxis behavior. Recently, Dey et al. reported a catalytic, self-propelled polymeric microsphere containing randomly distributed Pd NPs that showed pH taxis behavior as a result of an increase in the H_2O_2 decomposition rate with an increase in the pH value of the medium, which resulted in motion of the micromotor from the lower pH regions in the aqueous solutions towards the higher pH regions.[207]

3.5. Remediation Systems

Contamination caused by industrial and urban wastewater is a long-standing problem that has a high impact on the environment. The latest advances in MNMs are providing initial proof-of-concept applications towards environmental remediation, and have recently been reviewed.[186a,208] Table 2 summarizes the most significant reports of the use of MNMs for environmental applications. For example, MNMs can be used as environmental monitoring tools, by taking advantage of their chemical sensing capabilities (see Section 3.4). A chemical modification of the outer surface of MNMs with a self-assembled monolayer of hydrophobic compounds allows them to capture and transport oil droplets from contaminated waters, which has been demonstrated with microtubular motors[205] and Janus particles.[93] A further step in the field has been recently reported, with the first example of micromotors capable of oxidizing organic pollutants in aqueous solutions.[141a] Sanchez and co-workers designed Fe/Pt microtubular motors that possess double functionality, namely, catalytic self-propulsion achieved by H_2O_2 decomposition in the internal Pt layer and degradation of organic pollutants in solution as a result of the useful function of the Fe outer layer that enables Fenton reactions (Figure 25 A). The multifunctionality of these micromotors results in a synergistic effect that enhances water remediation, as a consequence of the combination of the degradation of pollutants and the active mixing of the treated solution. The importance of these findings has launched the idea of fabricating new designs of micromotors that can provide enhanced catalytic reactions based on their capacity to mix aqueous solutions. Almost simultaneously, Wang and co-workers illustrated the employment of PEDOT/Pt microtubular motors to boost the degradation of chemical threats (Figure 25 B).[186b] Briefly, the oxidation of an organophospate nerve agent by H_2O_2 was accelerated by the presence of the self-propelled micromotors, which contributed to an efficient

mixing of the treated aqueous solution without the need for external mechanical stirrers.

4. Outlook and Future Perspectives

Since the end of 1959, when Richard Feynman gave his visionary talk "There's plenty of room at the bottom",[5d] which kick-started the conceptual genesis of nanotechnology, much has been achieved in the field. The last two decades have seen a tremendous amount of work go into discovering new methods for nanostructure fabrication and application development. Initially, the field of MNMs included chemically propelled bimetallic nanorods, but has grown to incorporate various motor shapes and designs, various methods of motion control, and an impressive range of proof-of-concept applications. The self-propulsion of micro- and nanoscale devices without the use of external energy is an exciting concept by itself—but when able to perform advanced tasks such as the transport of cargo in a precise and selective manner, delivery to specific locations, chemical sensing, and environmental remediation—it takes us into an entirely new field with a lot of potential in multidisciplinary areas. The vision that intelligent MNMs could one day become powerful tools in biomedicine, cell engineering, and personalized healthcare has driven this field to new heights, but the ultimate dream, that is, in vivo biomedical applications, still remains to be achieved.

Nature can be a great source of inspiration for the design of these motors, as for billions of years it has built highly capable and efficient organisms which convert chemical energy into mechanical motion. Understanding their functions and capabilities plays an important role in the process of design. Artificial MNMs start from very simple structures so that the complexity of engineering at the microscale does not limit the development of the field. MNMs have been fabricated by a range of methods, from simple electrochemistry for nanowires to ones involving complicated clean-room set ups for microtubes. All of them have been elaborated to enable the readers to choose on the basis of their available facilities.

Different MNM designs have specific advantages and disadvantages. Nanowires, while extensively studied, have limitations for operating in high ionic media and generate low power. These constraints have been overcome by tubular micromotors which are highly versatile, adaptable for various applications, and possess greater power because of their size and bubble propulsion mechanism. The motion of Janus particles is easy to model because of their symmetric shape and they are widely used to demonstrate proof-of-concept applications. Simple modifications in these structures have given rise to new propulsion mechanisms and applications. A flexible nanowire can be magnetically propelled, one with a concave end by ultrasound, and immobilized microtubes can operate as micropumps.

It is clear that much work needs to be done to discover new MNM designs and discover new fields of applications for MNMs. The fuel has been a severe constraint for MNM systems. Commonly used chemicals such as H_2O_2 and hydrazine are not biocompatible and, therefore, limit possibilities in biomedical applications. Motors driven just by water have been described, but their lifetimes are short, which inhibits their use. To address this limitation there has been an effort to develop more efficient propulsion methods and other biocompatible sources of motion. For example, the use of enzymes or motile cells could give rise to biologically friendly MNMs.

Self-propelled motors, which cannot be controlled externally, are of little use for practical applications, and elaborate methods to control these motors have been developed. Systems which enable comprehensive spatial and temporal control of the MNMs through various techniques have been described. There are still challenges to build systems that enable more accurate control of the motion and ultimately to develop self-regulated motors guided by their fluid environment and which communicate between each other while simultaneously communicating with an external control.

The recently reported negligible toxicity of metallic tubular micromotors on human lung cell viability[209] is promising for in vivo applications. However, several issues need to be solved before scaling toward biomedical applications. For example, preventing the release of metallic ions into the surrounding solution because of corrosion of the MNMs,[210] and performing accurate studies of the effect of the accumulation of bubbles inside a living organism. While the quest for biocompatibility is a challenging and ongoing one, chemically propelled MNMs can still be used for a variety of other applications. The dynamic assembly of particles on the nanoscale, already observed in certain systems, can lead to functionalities that have so far been limited to biological systems. Collective motion, also ubiquitous in nature, can also be studied in MNM systems. These motors can be used for chemical sensing and for enhancing chemical reactions—both applications with great industrial potential. Environmental remediation by MNMs, already demonstrated at a foundational level, can have great implications on our fast degrading and depleting natural resources. Future research in the field of MNMs could be envisioned to occur in areas such as in energy harvesting, the production of electrical energy,[211] as well as in the generation of photocatalytic active sites to incorporate light-controlled motion of MNMs by photochemical reactions.[212] The incorporation of biocompatibility and accurate motion control into a single MNM is currently the largest challenge in the field, but the combination of biological motors and artificial microdevices could be one of the most promising synergies in future microrobotics.

We acknowledge financial support from the European Research Council under the European Union's Seventh Framework Programme (FP7/2007–2013)/ERC grant agreement [no. 311529] and the DFG Research Grants Programme (Grant SA 2525/1-1). We thank Kyoung Duck Seo for the frontispiece graphic and schemes. We thank S. Dietrich, J. G. Gibbs, X. Ma, M. N. Popescu, M. M. Stanton, and M. Tasinkevych for proof-reading the manuscript.

Received: June 10, 2014
Published online: December 12, 2014

[1] a) W. F. Paxton, K. C. Kistler, C. C. Olmeda, A. Sen, S. K. St Angelo, Y. Y. Cao, T. E. Mallouk, P. E. Lammert, V. H. Crespi, *J. Am. Chem. Soc.* **2004**, *126*, 13424 – 13431; b) S. Fournier-Bidoz, A. C. Arsenault, I. Manners, G. A. Ozin, *Chem. Commun.* **2005**, 441 – 443.

[2] R. F. Ismagilov, A. Schwartz, N. Bowden, G. M. Whitesides, *Angew. Chem. Int. Ed.* **2002**, *41*, 652 – 654; *Angew. Chem.* **2002**, *114*, 674 – 676.

[3] a) S. Nakata, K. Matsuo, *Langmuir* **2005**, *21*, 982 – 984; b) M. M. Hanczyc, T. Toyota, T. Ikegami, N. Packard, T. Sugawara, *J. Am. Chem. Soc.* **2007**, *129*, 9386 – 9391; c) R. Sharma, S. T. Chang, O. D. Velev, *Langmuir* **2012**, *28*, 10128 – 10135; d) G. J. Zhao, M. Pumera, *Chem. Asian J.* **2012**, *7*, 1994 – 2002.

[4] a) W. F. Paxton, A. Sen, T. E. Mallouk, *Chem. Eur. J.* **2005**, *11*, 6462 – 6470; b) W. F. Paxton, S. Sundararajan, T. E. Mallouk, A. Sen, *Angew. Chem. Int. Ed.* **2006**, *45*, 5420 – 5429; *Angew. Chem.* **2006**, *118*, 5546 – 5556; c) T. E. Mallouk, A. Sen, *Sci. Am.* **2009**, *300*, 72 – 77; d) S. Sánchez, M. Pumera, *Chem. Asian J.* **2009**, *4*, 1402 – 1410; e) J. Wang, *ACS Nano* **2009**, *3*, 4 – 9; f) D. Patra, S. Sengupta, W. T. Duan, H. Zhang, R. Pavlick, A. Sen, *Nanoscale* **2013**, *5*, 1273 – 1283; g) W. Wang, W. T. Duan, S. Ahmed, T. E. Mallouk, A. Sen, *Nano Today* **2013**, *8*, 531 – 554; h) K. E. Peyer, L. Zhang, B. J. Nelson, *Nanoscale* **2013**, *5*, 1259 – 1272; i) M. Guix, C. C. Mayorga-Martinez, A. Merkoci, *Chem. Rev.* **2014**, *114*, 6285 – 6322.

[5] a) F. Jian, C. S. Kwon, *Micromachines* **2014**, *5*, 97 – 113; b) J. Wang, W. Gao, *ACS Nano* **2012**, *6*, 5745 – 5751; c) J. Wang, *Nanomachines*: *Fundamentals and Applications*, Wiley-VCH, Weinheim, **2013**; d) R. P. Feynman in *Miniaturization* (Ed.: H. D. Gilbert), Reinhold, New York, **1961**, pp. 282 – 296.

[6] G. A. Ozin, I. Manners, S. Fournier-Bidoz, A. Arsenault, *Adv. Mater.* **2005**, *17*, 3011 – 3018.

[7] a) S. T. Chang, V. N. Paunov, D. N. Petsev, O. D. Velev, *Nat. Mater.* **2007**, *6*, 235 – 240; b) G. Loget, A. Kuhn, *Nat. Commun.* **2011**, *2*, 535; c) P. Calvo-Marzal, S. Sattayasamitsathit, S. Balasubramanian, J. R. Windmiller, C. Dao, J. Wang, *Chem. Commun.* **2010**, *46*, 1623 – 1624.

[8] a) A. Ghosh, P. Fischer, *Nano Lett.* **2009**, *9*, 2243 – 2245; b) S. Tottori, L. Zhang, F. M. Qiu, K. K. Krawczyk, A. Franco-Obregon, B. J. Nelson, *Adv. Mater.* **2012**, *24*, 811 – 816; c) W. Gao, D. Kagan, O. S. Pak, C. Clawson, S. Campuzano, E. Chuluun-Erdene, E. Shipton, E. E. Fullerton, L. F. Zhang, E. Lauga, J. Wang, *Small* **2012**, *8*, 460 – 467.

[9] a) W. Wang, L. A. Castro, M. Hoyos, T. E. Mallouk, *ACS Nano* **2012**, *6*, 6122 – 6132; b) W. Wang, S. X. Li, L. Mair, S. Ahmed, T. J. Huang, T. E. Mallouk, *Angew. Chem. Int. Ed.* **2014**, *53*, 3201 – 3204; *Angew. Chem.* **2014**, *126*, 3265 – 3268; c) V. Garcia-Gradilla, J. Orozco, S. Sattayasamitsathit, F. Soto, F. Kuralay, A. Pourazary, A. Katzenberg, W. Gao, Y. F. Shen, J. Wang, *ACS Nano* **2013**, *7*, 9232 – 9240.

[10] a) S. Babel, B. t. Hagen, H. Löwen, *J. Stat. Mech. Theor. Exp.* **2014**, P02011; b) J. A. Cohen, R. Golestanian, *Phys. Rev. Lett.* **2014**, *112*, 068302; c) R. Golestanian, *Phys. Rev. Lett.* **2009**, *102*, 188305; d) S. Saha, R. Golestanian, S. Ramaswamy, *Phys. Rev. E* **2014**, *89*, 062316.

[11] a) Y. Wang, S. T. Fei, Y. M. Byun, P. E. Lammert, V. H. Crespi, A. Sen, T. E. Mallouk, *J. Am. Chem. Soc.* **2009**, *131*, 9926 – 9927; b) M. Ibele, T. E. Mallouk, A. Sen, *Angew. Chem. Int. Ed.* **2009**, *48*, 3308 – 3312; *Angew. Chem.* **2009**, *121*, 3358 – 3362; c) M. E. Ibele, P. E. Lammert, V. H. Crespi, A. Sen, *ACS Nano* **2010**, *4*, 4845 – 4851; d) D. Kagan, S. Balasubramanian, J. Wang, *Angew. Chem. Int. Ed.* **2011**, *50*, 503 – 506; *Angew. Chem.* **2011**, *123*, 523 – 526; e) A. A. Solovev, S. Sanchez, O. G. Schmidt, *Nanoscale* **2013**, *5*, 1284 – 1293; f) Y. Hong, N. M. K. Blackman, N. D. Kopp, A. Sen, D. Velegol, *Phys. Rev. Lett.* **2007**, *99*, 178103; g) I. Theurkauff, C. Cottin-Bizonne, J. Palacci, C. Ybert, L. Bocquet, *Phys. Rev. Lett.* **2012**, *108*, 268303; h) J. Palacci, S. Sacanna, A. P. Steinberg, D. J. Pine, P. M. Chaikin, *Science* **2013**, *339*, 936 – 940; i) W. T. Duan, R. Liu, A. Sen, *J. Am. Chem. Soc.* **2013**, *135*, 1280 – 1283; j) L. Baraban, S. M. Harazim, S. Sanchez, O. G. Schmidt, *Angew. Chem. Int. Ed.* **2013**, *52*, 5552 – 5556; *Angew. Chem.* **2013**, *125*, 5662 – 5666; k) S. Hernàndez-Navarro, P. Tierno, J. Ignés-Mullol, F. Sagués, *Angew. Chem. Int. Ed.* **2014**, *53*, 1096 – 10700; *Angew. Chem.* **2014**, *126*, 10872 – 10876.

[12] W. Wang, T. Y. Chiang, D. Velegol, T. E. Mallouk, *J. Am. Chem. Soc.* **2013**, *135*, 10557 – 10565.

[13] E. M. Purcell, *Am. J. Phys.* **1977**, *45*, 3 – 11.

[14] A. Agarwal, H. Hess, *Prog. Polym. Sci.* **2010**, *35*, 252 – 277.

[15] A. Jannasch, V. Bormuth, M. Storch, J. Howard, E. Schäffer, *Biophys. J.* **2013**, *104*, 2456 – 2464.

[16] W. Qiu, N. D. Derr, B. S. Goodman, E. Villa, D. Wu, W. Shih, S. L. Reck-Peterson, *Nat. Struct. Mol. Biol.* **2012**, *19*, 193 – 200.

[17] a) S. Ramachandran, K. H. Ernst, G. D. Bachand, V. Vogel, H. Hess, *Small* **2006**, *2*, 330 – 334; b) H. Hess, J. Clemmens, D. Qin, J. Howard, V. Vogel, *Nano Lett.* **2001**, *1*, 235 – 239.

[18] a) H. Hess, C. M. Matzke, R. K. Doot, J. Clemmens, G. D. Bachand, B. C. Bunker, V. Vogel, *Nano Lett.* **2003**, *3*, 1651 – 1655; b) W. J. Walter, S. Diez, *Nat. Nanotechnol.* **2012**, *7*, 213 – 214; c) L. Chen, M. Nakamura, T. D. Schindler, D. Parker, Z. Bryant, *Nat. Nanotechnol.* **2012**, *7*, 252 – 256; d) A. Goel, V. Vogel, *Nat. Nanotechnol.* **2008**, *3*, 465 – 475; e) V. Schroeder, T. Korten, H. Linke, S. Diez, I. Maximov, *Nano Lett.* **2013**, *13*, 3434 – 3438; f) H. Hess in *Annu. Rev. Biomed. Eng.*, *Vol. 13* (Eds.: M. L. Yarmush, J. S. Duncan, M. L. Gray), Annual Reviews, Palo Alto, **2011**, pp. 429 – 450.

[19] T. Fischer, A. Agarwal, H. Hess, *Nat. Nanotechnol.* **2009**, *4*, 162 – 166.

[20] J. Bull, A. Hunt, E. Meyhöfer, *Biomed. Microdevices* **2005**, *7*, 21 – 33.

[21] T. Nitta, H. Hess, *Nano Lett.* **2005**, *5*, 1337 – 1342.

[22] H. S. Muddana, S. Sengupta, T. E. Mallouk, A. Sen, P. J. Butler, *J. Am. Chem. Soc.* **2010**, *132*, 2110 – 2111.

[23] H. Hess, G. D. Bachand, V. Vogel, *Chem. Eur. J.* **2004**, *10*, 2110 – 2116.

[24] S. Sanchez, A. A. Solovev, Y. Mei, O. G. Schmidt, *J. Am. Chem. Soc.* **2010**, *132*, 13144 – 13145.

[25] B. Behkam, M. Sitti, *Appl. Phys. Lett.* **2007**, *90*, 023902.

[26] R. Di Leonardo, L. Angelani, D. Dell′Arciprete, G. Ruocco, V. Iebba, S. Schippa, M. P. Conte, F. Mecarini, F. De Angelis, E. Di Fabrizio, *Proc. Natl. Acad. Sci. USA* **2010**, *107*, 9541 – 9545.

[27] S. Martel, *Biomed. Microdevices* **2012**, *14*, 1033 – 1045.

[28] V. Magdanz, S. Sanchez, O. G. Schmidt, *Adv. Mater.* **2013**, *25*, 6581 – 6588.

[29] J. C. Nawroth, H. Lee, A. W. Feinberg, C. M. Ripplinger, M. L. McCain, A. Grosberg, J. O. Dabiri, K. K. Parker, *Nat. Biotechnol.* **2012**, *30*, 792 – 797.

[30] S. Sengupta, K. K. Dey, H. S. Muddana, T. Tabouillot, M. E. Ibele, P. J. Butler, A. Sen, *J. Am. Chem. Soc.* **2013**, *135*, 1406 – 1414.

[31] R. K. Soong, G. D. Bachand, H. P. Neves, A. G. Olkhovets, H. G. Craighead, C. D. Montemagno, *Science* **2000**, *290*, 1555 – 1558.

[32] N. Mano, A. Heller, *J. Am. Chem. Soc.* **2005**, *127*, 11574 – 11575.

[33] D. Pantarotto, W. R. Browne, B. L. Feringa, *Chem. Commun.* **2008**, 1533 – 1535.

[34] J. Orozco, V. Garcia-Gradilla, M. D′Agostino, W. Gao, A. Cortes, J. Wang, *ACS Nano* **2013**, *7*, 818 – 824.

[35] J. Simmchen, A. Baeza, D. Ruiz, M. J. Esplandiu, M. Vallet-Regí, *Small* **2012**, *8*, 2053 – 2059.

[36] R. W. Carlsen, M. Sitti, *Small* **2014**, *10*, 3831 – 3851.

[37] S. J. Park, H. Bae, J. Kim, B. Lim, J. Park, S. Park, *Lab Chip* **2010**, *10*, 1706 – 1711.
[38] R. Fernandes, M. Zuniga, F. R. Sassine, M. Karakoy, D. H. Gracias, *Small* **2011**, *7*, 588 – 592.
[39] a) S. Martel in *Experimental Robotics*, *Vol. 79* (Eds.: O. Khatib, V. Kumar, G. Sukhatme), Springer, Berlin/Heidelberg, **2014**, pp. 775 – 784; b) S. Martel, O. Felfoul, J.-B. Mathieu, A. Chanu, S. Tamaz, M. Mohammadi, M. Mankiewicz, N. Tabatabaei, *Int. J. Robot. Res.* **2009**, *28*, 1169 – 1182.
[40] S. Sengupta, D. Patra, I. Ortiz-Rivera, A. Agrawal, S. Shklyaev, K. K. Dey, U. Cordova-Figueroa, T. E. Mallouk, A. Sen, *Nat. Chem.* **2014**, *6*, 415 – 422.
[41] N. Darnton, L. Turner, K. Breuer, H. C. Berg, *Biophys. J.* **2004**, *86*, 1863 – 1870.
[42] Y. Tanaka, K. Sato, T. Shimizu, M. Yamato, T. Okano, T. Kitamori, *Lab Chip* **2007**, *7*, 207 – 212.
[43] Y. N. Xia, P. D. Yang, Y. G. Sun, Y. Y. Wu, B. Mayers, B. Gates, Y. D. Yin, F. Kim, Y. Q. Yan, *Adv. Mater.* **2003**, *15*, 353 – 389.
[44] G. E. Possin, *Rev. Sci. Instrum.* **1970**, *41*, 772 – 774.
[45] D. Al-Mawlawi, C. Z. Liu, M. Moskovits, *J. Mater. Res.* **1994**, *9*, 1014 – 1018.
[46] B. R. Martin, D. J. Dermody, B. D. Reiss, M. M. Fang, L. A. Lyon, M. J. Natan, T. E. Mallouk, *Adv. Mater.* **1999**, *11*, 1021 – 1025.
[47] S. R. Nicewarner-Pena, R. G. Freeman, B. D. Reiss, L. He, D. J. Pena, I. D. Walton, R. Cromer, C. D. Keating, M. J. Natan, *Science* **2001**, *294*, 137 – 141.
[48] C. R. Martin, *Chem. Mater.* **1996**, *8*, 1739 – 1746.
[49] F. Müller, O. Jessensky, A.-P. Li, K. Nielsch, J. Choi, R. Ji, Max-Planck-Institut für Mikrostrukturphysik. http://www.mpi-halle.mpg.de/department2/research-areas/ordered-porous-materials/porous-alumina/abstract/self-organization-lithography/, **2007**.
[50] Y. Wang, R. M. Hernandez, D. J. Bartlett, Jr., J. M. Bingham, T. R. Kline, A. Sen, T. E. Mallouk, *Langmuir* **2006**, *22*, 10451 – 10456.
[51] W. Gao, K. M. Manesh, J. Hua, S. Sattayasamitsathit, J. Wang, *Small* **2011**, *7*, 2047 – 2051.
[52] T. Mirkovic, M. L. Foo, A. C. Arsenault, S. Fournier-Bidoz, N. S. Zacharia, G. A. Ozin, *Nat. Nanotechnol.* **2007**, *2*, 565 – 569.
[53] J. M. Catchmark, S. Subramanian, A. Sen, *Small* **2005**, *1*, 202 – 206.
[54] P. Dhar, T. M. Fischer, Y. Wang, T. E. Mallouk, W. F. Paxton, A. Sen, *Nano Lett.* **2006**, *6*, 66 – 72.
[55] T. Mirkovic, N. S. Zacharia, G. D. Scholes, G. A. Ozin, *Small* **2010**, *6*, 159 – 167.
[56] R. Laocharoensuk, J. Burdick, J. Wang, *ACS Nano* **2008**, *2*, 1069 – 1075.
[57] U. K. Demirok, R. Laocharoensuk, K. M. Manesh, J. Wang, *Angew. Chem. Int. Ed.* **2008**, *47*, 9349 – 9351; *Angew. Chem.* **2008**, *120*, 9489 – 9491.
[58] M. E. Ibele, Y. Wang, T. R. Kline, T. E. Mallouk, A. Sen, *J. Am. Chem. Soc.* **2007**, *129*, 7762 – 7763.
[59] R. Liu, A. Sen, *J. Am. Chem. Soc.* **2011**, *133*, 20064 – 20067.
[60] Z. Fattah, G. Loget, V. Lapeyre, P. Garrigue, C. Warakulwit, J. Limtrakul, L. Bouffier, A. Kuhn, *Electrochim. Acta* **2011**, *56*, 10562 – 10566.
[61] a) T. R. Kline, W. F. Paxton, T. E. Mallouk, A. Sen, *Angew. Chem. Int. Ed.* **2005**, *44*, 744 – 746; *Angew. Chem.* **2005**, *117*, 754 – 756; b) J. Burdick, R. Laocharoensuk, P. M. Wheat, J. D. Posner, J. Wang, *J. Am. Chem. Soc.* **2008**, *130*, 8164 – 8165; c) J. C. Love, A. R. Urbach, M. G. Prentiss, G. M. Whitesides, *J. Am. Chem. Soc.* **2003**, *125*, 12696 – 12697.
[62] S. Balasubramanian, D. Kagan, K. M. Manesh, P. Calvo-Marzal, G. U. Flechsig, J. Wang, *Small* **2009**, *5*, 1569 – 1574.
[63] P. Calvo-Marzal, K. M. Manesh, D. Kagan, S. Balasubramanian, M. Cardona, G. U. Flechsig, J. Posner, J. Wang, *Chem. Commun.* **2009**, 4509 – 4511.
[64] D. Kagan, P. Calvo-Marzal, S. Balasubramanian, S. Sattayasamitsathit, K. M. Manesh, G. U. Flechsig, J. Wang, *J. Am. Chem. Soc.* **2009**, *131*, 12082 – 12803.
[65] Y. P. He, J. S. Wu, Y. P. Zhao, *Nano Lett.* **2007**, *7*, 1369 – 1375.
[66] L. D. Qin, M. J. Banholzer, X. Y. Xu, L. Huang, C. A. Mirkin, *J. Am. Chem. Soc.* **2007**, *129*, 14870 – 14871.
[67] C. Casagrande, M. Veyssie, *C. R. Acad. Sci. Ser. II* **1988**, *306*, 1423 – 1425.
[68] P.-G. de Gennes, *Angew. Chem. Int. Ed. Engl.* **1992**, *31*, 842 – 845; *Angew. Chem.* **1992**, *104*, 856 – 859.
[69] a) H. Takei, N. Shimizu, *Langmuir* **1997**, *13*, 1865 – 1868; b) J. C. Love, B. D. Gates, D. B. Wolfe, K. E. Paul, G. M. Whitesides, *Nano Lett.* **2002**, *2*, 891 – 894; c) A. Perro, S. Reculusa, S. Ravaine, E. Bourgeat-Lami, E. Duguet, *J. Mater. Chem.* **2005**, *15*, 3745 – 3760; d) A. Walther, A. H. E. Muller, *Chem. Rev.* **2013**, *113*, 5194 – 5261; e) Y. Song, S. W. Chen, *Chem. Asian J.* **2014**, *9*, 418 – 430; f) X. Pang, C. Wan, M. Wang, Z. Lin, *Angew. Chem. Int. Ed.* **2014**, *53*, 5524 – 5538; *Angew. Chem.* **2014**, *126*, 5630 – 5644.
[70] a) B. V. Derjaguin, G. P. Sidorenkov, E. A. Zubashchenkov, E. V. Kiseleva, *Kolloidn. Zh.* **1947**, *9*, 335 – 347; b) J. L. Anderson, D. C. Prieve, *Sep. Purif. Rev.* **1984**, *13*, 67 – 103; c) J. L. Anderson, *Annu. Rev. Fluid Mech.* **1989**, *21*, 61 – 99.
[71] R. Golestanian, T. B. Liverpool, A. Ajdari, *Phys. Rev. Lett.* **2005**, *94*, 220801.
[72] J. R. Howse, R. A. Jones, A. J. Ryan, T. Gough, R. Vafabakhsh, R. Golestanian, *Phys. Rev. Lett.* **2007**, *99*, 048102.
[73] L. Baraban, D. Makarov, R. Streubel, I. Monch, D. Grimm, S. Sanchez, O. G. Schmidt, *ACS Nano* **2012**, *6*, 3383 – 3389.
[74] C. Kreuter, U. Siems, P. Nielaba, P. Leiderer, A. Erbe, *Eur. Phys. J. Spec. Top.* **2013**, *222*, 2923 – 2939.
[75] W. Gao, A. Pei, J. Wang, *ACS Nano* **2012**, *6*, 8432 – 8438.
[76] F. Z. Mou, C. R. Chen, H. R. Ma, Y. X. Yin, Q. Z. Wu, J. G. Guan, *Angew. Chem. Int. Ed.* **2013**, *52*, 7208 – 7212; *Angew. Chem.* **2013**, *125*, 7349 – 7353.
[77] W. Gao, A. Pei, R. F. Dong, J. Wang, *J. Am. Chem. Soc.* **2014**, *136*, 2276 – 2279.
[78] G. Loget, J. Roche, A. Kuhn, *Adv. Mater.* **2012**, *24*, 5111 – 5116.
[79] T.-C. Lee, M. Alarcón-Correa, C. Miksch, K. Hahn, J. G. Gibbs, P. Fischer, *Nano Lett.* **2014**, *14*, 2407 – 2412.
[80] R. Glass, M. Moller, J. P. Spatz, *Nanotechnology* **2003**, *14*, 1153 – 1160.
[81] a) K. Robbie, M. J. Brett, *J. Vac. Sci. Technol. A* **1997**, *15*, 1460 – 1465; b) Y. P. Zhao, D. X. Ye, G. C. Wang, T. M. Lu, *Nano Lett.* **2002**, *2*, 351 – 354.
[82] M. Xuan, J. Shao, X. Lin, L. Dai, Q. He, *ChemPhysChem* **2014**, *15*, 2255 – 2260.
[83] S. Huh, J. W. Wiench, J. C. Yoo, M. Pruski, V. S. Y. Lin, *Chem. Mater.* **2003**, *15*, 4247 – 4256.
[84] J. G. Gibbs, N. A. Fragnito, Y. P. Zhao, *Appl. Phys. Lett.* **2010**, *97*, 253107.
[85] a) J. G. Gibbs, Y. P. Zhao, *Small* **2010**, *6*, 1656 – 1662; b) J. G. Gibbs, Y. P. Zhao, *Small* **2009**, *5*, 2304 – 2308.
[86] W. J. Huang, M. Manjare, Y. P. Zhao, *J. Phys. Chem. C* **2013**, *117*, 21590 – 21596.
[87] P. Tierno, R. Albalat, F. Sagues, *Small* **2010**, *6*, 1749 – 1752.
[88] L. F. Valadares, Y.-G. Tao, N. S. Zacharia, V. Kitaev, F. Galembeck, R. Kapral, G. A. Ozin, *Small* **2010**, *6*, 565 – 572.
[89] Y. Y. Hong, D. Velegol, N. Chaturvedi, A. Sen, *Phys. Chem. Chem. Phys.* **2010**, *12*, 1423 – 1435.
[90] S. Wang, N. Wu, *Langmuir* **2014**, *30*, 3477 – 3486.
[91] D. A. Wilson, R. J. M. Nolte, J. C. M. van Hest, *Nat. Chem.* **2012**, *4*, 268 – 274.
[92] W. Gao, M. D'Agostino, V. Garcia-Gradilla, J. Orozco, J. Wang, *Small* **2013**, *9*, 467 – 471.
[93] W. Gao, X. M. Feng, A. Pei, Y. E. Gu, J. X. Li, J. Wang, *Nanoscale* **2013**, *5*, 4696 – 4700.

[94] A. Sen, M. Ibele, Y. Hong, D. Velegol, *Faraday Discuss.* **2009**, *143*, 15 – 27.
[95] H. Ke, S. R. Ye, R. L. Carroll, K. Showalter, *J. Phys. Chem. A* **2010**, *114*, 5462 – 5467.
[96] S. Ebbens, R. A. L. Jones, A. J. Ryan, R. Golestanian, J. R. Howse, *Phys. Rev. E* **2010**, *82*, 015304.
[97] S. J. Ebbens, J. R. Howse, *Langmuir* **2011**, *27*, 12293 – 12296.
[98] R. A. Pavlick, S. Sengupta, T. McFadden, H. Zhang, A. Sen, *Angew. Chem. Int. Ed.* **2011**, *50*, 9374 – 9377; *Angew. Chem.* **2011**, *123*, 9546 – 9549.
[99] S. Ebbens, M. H. Tu, J. R. Howse, R. Golestanian, *Phys. Rev. E* **2012**, *85*, 020401.
[100] L. Baraban, M. Tasinkevych, M. N. Popescu, S. Sanchez, S. Dietrich, O. G. Schmidt, *Soft Matter* **2012**, *8*, 48 – 52.
[101] L. Baraban, D. Makarov, O. G. Schmidt, G. Cuniberti, P. Leiderer, A. Erbe, *Nanoscale* **2013**, *5*, 1332 – 1336.
[102] A. I. Campbell, S. J. Ebbens, *Langmuir* **2013**, *29*, 14066 – 14073.
[103] H. Zhang, W. T. Duan, L. Liu, A. Sen, *J. Am. Chem. Soc.* **2013**, *135*, 15734 – 15737.
[104] X. Zheng, B. ten Hagen, A. Kaiser, M. L. Wu, H. H. Cui, Z. Silber-Li, H. Lowen, *Phys. Rev. E* **2013**, *88*, 032304.
[105] M. L. Wu, H. Y. Zhang, X. Zheng, H. H. Cui, *AIP Adv.* **2014**, *4*, 031326.
[106] J. Simmchen, V. Magdanz, S. Sanchez, S. Chokmaviroj, D. Ruiz-Molina, A. Baeza, O. G. Schmidt, *RSC Adv.* **2014**, *4*, 20334 – 20340.
[107] J. L. Chen, H. Y. Zhang, X. Zheng, H. H. Cui, *AIP Adv.* **2014**, *4*, 031325.
[108] P. M. Wheat, N. A. Marine, J. L. Moran, J. D. Posner, *Langmuir* **2010**, *26*, 13052 – 13055.
[109] A. Brown, W. Poon, *Soft Matter* **2014**, *10*, 4016 – 4027.
[110] S. Ebbens, D. A. Gregory, G. Dunderdale, J. R. Howse, Y. Ibrahim, T. B. Liverpool, R. Golestanian, *Europhys. Lett.* **2014**, *106*, 58003.
[111] A. Agrawal, K. K. Dey, A. Paul, S. Basu, A. Chattopadhyay, *J. Phys. Chem. C* **2008**, *112*, 2797 – 2801.
[112] J. G. Gibbs, Y. P. Zhao, *Appl. Phys. Lett.* **2009**, *94*, 163104.
[113] M. Manjare, B. Yang, Y. P. Zhao, *Phys. Rev. Lett.* **2012**, *109*, 128305.
[114] Y. J. Wu, Z. G. Wu, X. K. Lin, Q. He, J. B. Li, *ACS Nano* **2012**, *6*, 10910 – 10916.
[115] B.-E. Pinchasik, H. Möhwald, A. G. Skirtach, *Small* **2014**, *10*, 2670 – 2677.
[116] J. Vicario, R. Eelkema, W. R. Browne, A. Meetsma, R. M. La Crois, B. L. Feringa, *Chem. Commun.* **2005**, 3936 – 3938.
[117] H. Wang, G. J. Zhao, M. Pumera, *J. Am. Chem. Soc.* **2014**, *136*, 2719 – 2722.
[118] a) M. N. Popescu, S. Dietrich, G. Oshanin, *J. Chem. Phys.* **2009**, *130*, 194702; b) W. E. Uspal, M. N. Popescu, S. Dietrich, M. Tasinkevych, *arXiv* **2014**, 1407.3216v1401 [cond-mat.soft].
[119] M. N. Popescu, M. Tasinkevych, S. Dietrich, *Europhys. Lett.* **2011**, *95*, 28004.
[120] M. N. Popescu, S. Dietrich, M. Tasinkevych, J. Ralston, *Eur. Phys. J. E* **2010**, *31*, 351 – 367.
[121] a) M. Albrecht, G. H. Hu, I. L. Guhr, T. C. Ulbrich, J. Boneberg, P. Leiderer, G. Schatz, *Nat. Mater.* **2005**, *4*, 203 – 206; b) T. C. Ulbrich, C. Bran, D. Makarov, O. Hellwig, J. D. Risner-Jamtgaard, D. Yaney, H. Rohrmann, V. Neu, M. Albrecht, *Phys. Rev. B* **2010**, *81*, 054421.
[122] H.-R. Jiang, N. Yoshinaga, M. Sano, *Phys. Rev. Lett.* **2010**, *105*, 268302.
[123] B. Qian, D. Montiel, A. Bregulla, F. Cichos, H. Yang, *Chem. Sci.* **2013**, *4*, 1420 – 1429.
[124] G. Loget, A. Kuhn, *Discovering the Future of Molecular Sciences* (Ed.: B. Pignataro), Wiley-VCH, Weinheim, **2014**, pp. 349 – 378.
[125] S. J. Wang, F. D. Ma, H. Zhao, N. Wu, *ACS Appl. Mater. Interfaces* **2014**, *6*, 4560 – 4569.
[126] G. Volpe, I. Buttinoni, D. Vogt, H. J. Kummerer, C. Bechinger, *Soft Matter* **2011**, *7*, 8810 – 8815.
[127] I. Buttinoni, G. Volpe, F. Kümmel, G. Volpe, C. Bechinger, *J. Phys. Condens. Matter* **2012**, *24*, 284129.
[128] M. S. Baker, V. Yadav, A. Sen, S. T. Phillips, *Angew. Chem. Int. Ed.* **2013**, *52*, 10295 – 10299; *Angew. Chem.* **2013**, *125*, 10485 – 10489.
[129] A. A. Solovev, Chemnitz University of Technology (Chemnitz, Germany), **2012**.
[130] S. Harazim, Chemnitz University of Technology (Chemnitz, Germany), **2012**.
[131] A. A. Solovev, Y. F. Mei, E. B. Urena, G. S. Huang, O. G. Schmidt, *Small* **2009**, *5*, 1688 – 1692.
[132] S. M. Harazim, W. Xi, C. K. Schmidt, S. Sanchez, O. G. Schmidt, *J. Mater. Chem.* **2012**, *22*, 2878 – 2884.
[133] Y. F. Mei, G. S. Huang, A. A. Solovev, E. B. Urena, I. Moench, F. Ding, T. Reindl, R. K. Y. Fu, P. K. Chu, O. G. Schmidt, *Adv. Mater.* **2008**, *20*, 4085 – 4090.
[134] O. G. Schmidt, K. Eberl, *Nature* **2001**, *410*, 168 – 168.
[135] a) C. S. Martinez-Cisneros, S. Sanchez, W. Xi, O. G. Schmidt, *Nano Lett.* **2014**, *14*, 2219 – 2224; b) C. C. B. Bufon, J. D. A. Espinoza, D. J. Thurmer, M. Bauer, C. Deneke, U. Zschieschang, H. Klauk, O. G. Schmidt, *Nano Lett.* **2011**, *11*, 3727 – 3733; c) D. Grimm, C. C. B. Bufon, C. Deneke, P. Atkinson, D. J. Thurmer, F. Schaffel, S. Gorantla, A. Bachmatiuk, O. G. Schmidt, *Nano Lett.* **2013**, *13*, 213 – 218; d) D. J. Thurmer, C. C. B. Bufon, C. Deneke, O. G. Schmidt, *Nano Lett.* **2010**, *10*, 3704 – 3709.
[136] V. Linder, B. D. Gates, D. Ryan, B. A. Parviz, G. M. Whitesides, *Small* **2005**, *1*, 730 – 736.
[137] a) V. Magdanz, G. Stoychev, L. Ionov, S. Sanchez, O. G. Schmidt, *Angew. Chem. Int. Ed.* **2014**, *53*, 2673 – 2677; *Angew. Chem.* **2014**, *126*, 2711 – 2715; b) G. Stoychev, S. Turcaud, J. W. C. Dunlop, L. Ionov, *Adv. Funct. Mater.* **2013**, *23*, 2295 – 2300; c) W. Xi, C. K. Schmidt, S. Sanchez, D. H. Gracias, R. E. Carazo-Salas, S. P. Jackson, O. G. Schmidt, *Nano Lett.* **2014**, 14, 4197 – 4202.
[138] a) N. Bassik, A. Brafman, A. M. Zarafshar, M. Jamal, D. Luvsanjav, F. M. Selaru, D. H. Gracias, *J. Am. Chem. Soc.* **2010**, *132*, 16314 – 16317; b) J. S. Randhawa, T. G. Leong, N. Bassik, B. R. Benson, M. T. Jochmans, D. H. Gracias, *J. Am. Chem. Soc.* **2008**, *130*, 17238 – 17239.
[139] S. Sanchez, A. N. Ananth, V. M. Fomin, M. Viehrig, O. G. Schmidt, *J. Am. Chem. Soc.* **2011**, *133*, 14860 – 14863.
[140] S. Sanchez, A. A. Solovev, S. M. Harazim, O. G. Schmidt, *J. Am. Chem. Soc.* **2011**, *133*, 701 – 703.
[141] a) L. Soler, V. Magdanz, V. M. Fomin, S. Sanchez, O. G. Schmidt, *ACS Nano* **2013**, *7*, 9611 – 9620; b) L. Soler, C. Martinez-Cisneros, A. Swiersy, S. Sanchez, O. G. Schmidt, *Lab Chip* **2013**, *13*, 4299 – 4303.
[142] S. Sanchez, A. A. Solovev, S. M. Harazim, C. Deneke, Y. F. Mei, O. G. Schmidt, *Chem. Rec.* **2011**, *11*, 367 – 370.
[143] A. A. Solovev, W. Xi, D. H. Gracias, S. M. Harazim, C. Deneke, S. Sanchez, O. G. Schmidt, *ACS Nano* **2012**, *6*, 1751 – 1756.
[144] G. J. Zhao, A. Ambrosi, M. Pumera, *J. Mater. Chem. A* **2014**, *2*, 1219 – 1223.
[145] K. Yao, M. Manjare, C. A. Barrett, B. Yang, T. T. Salguero, Y. Zhao, *J. Phys. Chem. Lett.* **2012**, *3*, 2204 – 2208.
[146] J. X. Li, J. Zhang, W. Gao, G. S. Huang, Z. F. Di, R. Liu, J. Wang, Y. F. Mei, *Adv. Mater.* **2013**, *25*, 3715 – 3721.
[147] J. Li, Z. Liu, G. Huang, Z. An, G. Chen, J. Zhang, M. Li, R. Liu, Y. Mei, *NPG Asia Mater.* **2014**, *6*, e94.
[148] a) G. J. Zhao, A. Ambrosi, M. Pumera, *Nanoscale* **2013**, *5*, 1319 – 1324; b) W. Gao, S. Sattayasamitsathit, J. Orozco, J. Wang, *J. Am. Chem. Soc.* **2011**, *133*, 11862 – 11864.

[149] W. Gao, S. Sattayasamitsathit, A. Uygun, A. Pei, A. Ponedal, J. Wang, *Nanoscale* **2012**, *4*, 2447 – 2453.
[150] J. Orozco, A. Cortes, G. Z. Cheng, S. Sattayasamitsathit, W. Gao, X. M. Feng, Y. F. Shen, J. Wang, *J. Am. Chem. Soc.* **2013**, *135*, 5336 – 5339.
[151] W. Gao, A. Uygun, J. Wang, *J. Am. Chem. Soc.* **2012**, *134*, 897 – 900.
[152] G. J. Zhao, M. Pumera, *RSC Adv.* **2013**, *3*, 3963 – 3966.
[153] a) A. A. Solovev, S. Sanchez, M. Pumera, Y. F. Mei, O. G. Schmidt, *Adv. Funct. Mater.* **2010**, *20*, 2430 – 2435; b) Y. F. Mei, A. A. Solovev, S. Sanchez, O. G. Schmidt, *Chem. Soc. Rev.* **2011**, *40*, 2109 – 2119.
[154] G. J. Zhao, M. Viehrig, M. Pumera, *Lab Chip* **2013**, *13*, 1930 – 1936.
[155] G. J. Zhao, N. T. Nguyen, M. Pumera, *Nanoscale* **2013**, *5*, 7277 – 7283.
[156] H. Wang, G. J. Zhao, M. Pumera, *Electrochem. Commun.* **2014**, *38*, 128 – 130.
[157] H. Wang, G. J. Zhao, M. Pumera, *Chem. Eur. J.* **2013**, *19*, 16756 – 16759.
[158] G. J. Zhao, S. Sanchez, O. G. Schmidt, M. Pumera, *Nanoscale* **2013**, *5*, 2909 – 2914.
[159] H. Wang, G. J. Zhao, M. Pumera, *Phys. Chem. Chem. Phys.* **2013**, *15*, 17277 – 17280.
[160] a) G. J. Zhao, H. Wang, B. Khezri, R. D. Webster, M. Pumera, *Lab Chip* **2013**, *13*, 2937 – 2941; b) W. Gao, S. Sattayasamitsathit, J. Orozco, J. Wang, *Nanoscale* **2013**, *5*, 8909 – 8914.
[161] H. Wang, G. J. Zhao, M. Pumera, *J. Phys. Chem. C* **2014**, *118*, 5268 – 5274.
[162] M. Manjare, B. Yang, Y. P. Zhao, *J. Phys. Chem. C* **2013**, *117*, 4657 – 4665.
[163] J. Li, G. Huang, M. Ye, M. Li, R. Liu, Y. Mei, *Nanoscale* **2011**, *3*, 5083 – 5089.
[164] V. M. Fomin, M. Hippler, V. Magdanz, L. Soler, S. Sanchez, O. G. Schmidt, *IEEE Trans. Robot.* **2014**, *30*, 40 – 48.
[165] L. Li, J. Wang, T. Li, W. Song, G. Zhang, *Soft Matter* **2014**, 10, 7511 – 7518.
[166] a) I. S. M. Khalil, V. Magdanz, S. Sanchez, O. G. Schmidt, S. Misra, *2013 IEEE/RSJ International Conference on Intelligent Robots and Systems* (Ed.: N. Amato), IEEE, New York, **2013**, pp. 2035 – 2040; b) I. S. M. Khalil, V. Magdanz, S. Sanchez, O. G. Schmidt, S. Misra, *IEEE Trans. Robot.* **2014**, *30*, 49 – 58; c) I. S. M. Khalil, V. Magdanz, S. Sanchez, O. G. Schmidt, S. Misra, *Plos One* **2014**, *9*, e83053.
[167] I. S. M. Khalil, V. Magdanz, S. Sanchez, O. G. Schmidt, S. Misra, *Appl. Phys. Lett.* **2013**, *103*, 172404.
[168] A. A. Solovev, E. J. Smith, C. C. B. Bufon, S. Sanchez, O. G. Schmidt, *Angew. Chem. Int. Ed.* **2011**, *50*, 10875 – 10878; *Angew. Chem.* **2011**, *123*, 11067 – 11070.
[169] L. Restrepo-Pérez, L. Soler, C. S. Martínez-Cisneros, S. Sánchez, O. G. Schmidt, *Lab Chip* **2014**, *14*, 1515 – 1518.
[170] T. Xu, F. Soto, W. Gao, V. Garcia-Gradilla, J. Li, X. Zhang, J. Wang, *J. Am. Chem. Soc.* **2014**, *136*, 8552 – 8555.
[171] A. Kaiser, H. H. Wensink, H. Löwen, *Phys. Rev. Lett.* **2012**, *108*, 268307.
[172] a) S. E. Hulme, W. R. DiLuzio, S. S. Shevkoplyas, L. Turner, M. Mayer, H. C. Berg, G. M. Whitesides, *Lab Chip* **2008**, *8*, 1888 – 1895; b) I. Berdakin, Y. Jeyaram, V. V. Moshchalkov, L. Venken, S. Dierckx, S. J. Vanderleyden, A. V. Silhanek, C. A. Condat, V. I. Marconi, *Phys. Rev. E* **2013**, *87*, 052702; c) I. Berdakin, A. V. Silhanek, H. N. M. Cortez, V. I. Marconi, C. A. Condat, *Cent. Eur. J. Phys.* **2013**, *11*, 1653 – 1661; d) A. Guidobaldi, Y. Jeyaram, I. Berdakin, V. V. Moshchalkov, C. A. Condat, V. I. Marconi, L. Giojalas, A. V. Silhanek, *Phys. Rev. E* **2014**, *89*, 032720.
[173] L. Restrepo-Pérez, L. Soler, C. S. Martínez-Cisneros, S. Sánchez, O. G. Schmidt, *Lab Chip* **2014**, *14*, 2914 – 2917.
[174] S. Sundararajan, P. E. Lammert, A. W. Zudans, V. H. Crespi, A. Sen, *Nano Lett.* **2008**, *8*, 1271 – 1276.
[175] S. Sundararajan, S. Sengupta, M. E. Ibele, A. Sen, *Small* **2010**, *6*, 1479 – 1482.
[176] D. Kagan, R. Laocharoensuk, M. Zimmerman, C. Clawson, S. Balasubramanian, D. Kong, D. Bishop, S. Sattayasamitsathit, L. F. Zhang, J. Wang, *Small* **2010**, *6*, 2741 – 2747.
[177] S. Sanchez, A. A. Solovev, S. Schulze, O. G. Schmidt, *Chem. Commun.* **2011**, *47*, 698 – 700.
[178] a) G. J. Zhao, S. Sanchez, O. G. Schmidt, M. Pumera, *Chem. Commun.* **2012**, *48*, 10090 – 10092; b) G. J. Zhao, H. Wang, S. Sanchez, O. G. Schmidt, M. Pumera, *Chem. Commun.* **2013**, *49*, 5147 – 5149.
[179] S. Campuzano, D. Kagan, J. Orozco, J. Wang, *Analyst* **2011**, *136*, 4621 – 4630.
[180] D. Kagan, S. Campuzano, S. Balasubramanian, F. Kuralay, G. U. Flechsig, J. Wang, *Nano Lett.* **2011**, *11*, 2083 – 2087.
[181] J. Orozco, S. Campuzano, D. Kagan, M. Zhou, W. Gao, J. Wang, *Anal. Chem.* **2011**, *83*, 7962 – 7969.
[182] S. Balasubramanian, D. Kagan, C. M. J. Hu, S. Campuzano, M. J. Lobo-Castanon, N. Lim, D. Y. Kang, M. Zimmerman, L. F. Zhang, J. Wang, *Angew. Chem. Int. Ed.* **2011**, *50*, 4161 – 4164; *Angew. Chem.* **2011**, *123*, 4247 – 4250.
[183] S. Campuzano, J. Orozco, D. Kagan, M. Guix, W. Gao, S. Sattayasamitsathit, J. C. Claussen, A. Merkoci, J. Wang, *Nano Lett.* **2012**, *12*, 396 – 401.
[184] F. Kuralay, S. Sattayasamitsathit, W. Gao, A. Uygun, A. Katzenberg, J. Wang, *J. Am. Chem. Soc.* **2012**, *134*, 15217 – 15220.
[185] M. García, J. Orozco, M. Guix, W. Gao, S. Sattayasamitsathit, A. Escarpa, A. Merkoci, J. Wang, *Nanoscale* **2013**, *5*, 1325 – 1331.
[186] a) L. Soler, S. Sanchez, *Nanoscale* **2014**, *6*, 7175 – 7182; b) J. Orozco, G. Z. Cheng, D. Vilela, S. Sattayasamitsathit, R. Vazquez-Duhalt, G. Valdes-Ramirez, O. S. Pak, A. Escarpa, C. Y. Kan, J. Wang, *Angew. Chem. Int. Ed.* **2013**, *52*, 13276 – 13279; *Angew. Chem.* **2013**, *125*, 13518 – 13521; c) J. Orozco, B. Jurado-Sánchez, G. Wagner, W. Gao, R. Vazquez-Duhalt, S. Sattayasamitsathit, M. Galarnyk, A. Cortés, D. Saintillan, J. Wang, *Langmuir* **2014**, *30*, 5082 – 5087.
[187] E. Morales-Narváez, M. Guix, M. Medina-Sánchez, C. C. Mayorga-Martinez, A. Merkoçi, *Small* **2014**, *10*, 2542 – 2548.
[188] W. Xi, A. A. Solovev, A. N. Ananth, D. H. Gracias, S. Sanchez, O. G. Schmidt, *Nanoscale* **2013**, *5*, 1294 – 1297.
[189] D. Kagan, M. J. Benchimol, J. C. Claussen, E. Chuluun-Erdene, S. Esener, J. Wang, *Angew. Chem. Int. Ed.* **2012**, *51*, 7519 – 7522; *Angew. Chem.* **2012**, *124*, 7637 – 7640.
[190] T. G. Leong, C. L. Randall, B. R. Benson, N. Bassik, G. M. Stern, D. H. Gracias, *Proc. Natl. Acad. Sci. USA* **2009**, *106*, 703 – 708.
[191] R. Mhanna, F. Qiu, L. Zhang, Y. Ding, K. Sugihara, M. Zenobi-Wong, B. J. Nelson, *Small* **2014**, *10*, 1953 – 1957.
[192] M. A. Zeeshan, S. Pane, S. K. Youn, E. Pellicer, S. Schuerle, J. Sort, S. Fusco, A. M. Lindo, H. G. Park, B. J. Nelson, *Adv. Funct. Mater.* **2013**, *23*, 823 – 831.
[193] S. Ahmed, W. Wang, L. O. Mair, R. D. Fraleigh, S. X. Li, L. A. Castro, M. Hoyos, T. J. Huang, T. E. Mallouk, *Langmuir* **2013**, *29*, 16113 – 16118.
[194] V. Yadav, J. D. Freedman, M. Grinstaff, A. Sen, *Angew. Chem. Int. Ed.* **2013**, *52*, 10997 – 11001; *Angew. Chem.* **2013**, *125*, 11203 – 11207.
[195] a) L. Abdelmohsen, F. Peng, Y. F. Tu, D. A. Wilson, *J. Mater. Chem. B* **2014**, *2*, 2395 – 2408; b) W. Gao, J. Wang, *Nanoscale* **2014**, *6*, 10486 – 10494.
[196] T. R. Kline, W. F. Paxton, Y. Wang, D. Velegol, T. E. Mallouk, A. Sen, *J. Am. Chem. Soc.* **2005**, *127*, 17150 – 17151.

[197] A. A. Farniya, M. J. Esplandiu, D. Reguera, A. Bachtold, *Phys. Rev. Lett.* **2013**, *111*, 168301.
[198] V. Yadav, H. Zhang, R. Pavlick, A. Sen, *J. Am. Chem. Soc.* **2012**, *134*, 15688 – 15691.
[199] A. A. Solovev, S. Sanchez, Y. F. Mei, O. G. Schmidt, *Phys. Chem. Chem. Phys.* **2011**, *13*, 10131 – 10135.
[200] H. Zhang, K. Yeung, J. S. Robbins, R. A. Pavlick, M. Wu, R. Liu, A. Sen, S. T. Phillips, *Angew. Chem. Int. Ed.* **2012**, *51*, 2400 – 2404; *Angew. Chem.* **2012**, *124*, 2450 – 2454.
[201] I.-K. Jun, H. Hess, *Adv. Mater.* **2010**, *22*, 4823 – 4825.
[202] J. Wu, S. Balasubramanian, D. Kagan, K. M. Manesh, S. Campuzano, J. Wang, *Nat. Commun.* **2010**, *1*, 36.
[203] M. Zhang, X. Xie, M. Tang, C. S. Criddle, Y. Cui, S. X. Wang, *Nat. Commun.* **2013**, *4*, 1866.
[204] G. Zhao, T. H. Seah, M. Pumera, *Chem. Eur. J.* **2011**, *17*, 12020 – 12026.
[205] M. Guix, J. Orozco, M. Garcia, W. Gao, S. Sattayasamitsathit, A. Merkoci, A. Escarpa, J. Wang, *ACS Nano* **2012**, *6*, 4445 – 4451.
[206] J. G. S. Moo, H. Wang, G. J. Zhao, M. Pumera, *Chem. Eur. J.* **2014**, *20*, 4292 – 4296.
[207] K. K. Dey, S. Bhandari, D. Bandyopadhyay, S. Basu, A. Chattopadhyay, *Small* **2013**, *9*, 1916 – 1920.
[208] W. Gao, J. Wang, *ACS Nano* **2014**, *8*, 3170 – 3180.
[209] E. L. K. Chng, G. J. Zhao, M. Pumera, *Nanoscale* **2014**, *6*, 2119 – 2124.
[210] G. J. Zhao, B. Khezri, S. Sanchez, O. G. Schmidt, R. D. Webster, M. Pumera, *Chem. Commun.* **2013**, *49*, 9125 – 9127.
[211] S. K. Sailapu, A. Chattopadhyay, *Angew. Chem. Int. Ed.* **2014**, *53*, 1521 – 1524; *Angew. Chem.* **2014**, *126*, 1547 – 1550.
[212] S. Giudicatti, S. M. Marz, L. Soler, A. Madani, M. R. Jorgensen, S. Sanchez, O. G. Schmidt, *J. Mater. Chem. C* **2014**, *2*, 5892 – 5901.